



Supporting Information

Palladium-Catalyzed Directed *meta*-Selective C–H Allylation of Arenes: Unactivated Internal Olefins as Allyl Surrogates

Tapas Kumar Achar⁺, Xinglong Zhang⁺, Rahul Mondal, M. S. Shanavas, Siddhartha Maiti, Sabyasachi Maity, Nityananda Pal, Robert S. Paton,* and Debabrata Maiti*

anie_201904608_sm_miscellaneous_information.pdf

Supporting Information
©Wiley-VCH 2016
69451 Weinheim, Germany

Palladium-Catalyzed Directed *meta*-Selective C–H Allylation of Arenes: Unactivated Internal Olefins as Allyl Surrogates

Tapas Kumar Achar,^{[a],†} Xinglong Zhang,^{[b],†} Rahul Mondal,^[a] Shanavas M. S.,^[a] Siddhartha Maiti,^[c] Sabyasachi Maity,^[a] Nityananda Pal,^[a] Robert S. Paton,^{*[b]} and Debabrata Maiti^{*[a]}

^[a]Department of Chemistry, Indian Institute of Technology Bombay, Powai, Mumbai 400076, India

^[b]Chemistry Research Laboratory, University of Oxford, Mansfield Road, Oxford OX1 3TA, United Kingdom

^[c]BSBE, Indian Institute of Technology Bombay, Powai, Mumbai 400076, India

† These authors contributed equally.

* Debabrata Maiti: dmaiti@chem.iitb.ac.in

* Robert S. Paton: robert.paton@colostate.edu

Abstract: Palladium(II)-catalyzed *meta*-selective C–H allylation of arenes has been developed utilizing synthetically inert unactivated acyclic internal olefins as allylic surrogates. The strong σ-donating and π-accepting ability of pyrimidine-based directing group facilitates the olefin insertion by overcoming inertness of the typical unactivated internal olefins. Exclusive allyl over styrenyl product selectivity as well as *E*-stereoselectivity were achieved with broad substrate scope, wide functional group tolerance and good to excellent yields. Late-stage functionalisations of pharmaceuticals were demonstrated. Experimental and computational studies shed insights on the mechanism and pointed to key palladacyclic steric control in determining product selectivities.

2.9. Computational Methods

Density functional theory (DFT) calculations were performed with *Gaussian 16* rev. A.03.¹ Geometry optimisations were carried out using recently developed global-hybrid meta-NGA (nonseparable gradient approximation) MN15 functional² with a mixed Karlsruhe-family basis set of triple- ζ valence def2-TZVPPD (where ‘D’ indicates diffuse basis functions) for Pd³ atom and def2-SVP^{4,5} for all other atoms (BS1). This functional was chosen as it performs much better than many other functionals in predicting transition metal reaction barrier heights.² Previously, Pd(II)-catalysed C-C bond formations have been studied using other functionals including meta-GGA TPSS and range-separated ω B97X-D functionals.^{6,7} MN15 has been shown to give better agreement in geometry predictions of both transition metal complex and organic molecules than many other functionals including ω B97X-D and TPSS.² Minima and transition structures on the potential energy surface (PES) were confirmed as such by harmonic frequency analysis, showing respectively zero and one imaginary frequency, at the same level of theory. Single point (SP) corrections were performed separately with either MN15 or ω B97X-D⁸ functional and def2-QZVPP⁴ basis set for all atoms. The SMD continuum solvation model⁹ was carried out to include the effect of acetonitrile solvent on the computed Gibbs energy profile. Gibbs energies were evaluated at 363.15 K, using a quasi-RRHO treatment of vibrational entropies.^{10,11} Vibrational entropies of frequencies below 100 cm⁻¹ were obtained according to a free rotor description, using a smooth damping function to interpolate between the two limiting descriptions. The free energies were further corrected using standard concentration of 1 mol/L, which were used in solvation calculations. SMD(acetonitrile)- ω B97X-D/def2-QZVPP//MN15/BS1 Gibbs energies were given with SMD(acetonitrile)-MN15/def2-QZVPP//MN15/BS1 Gibbs energies given in brackets throughout. All values are quoted in kcal mol⁻¹.

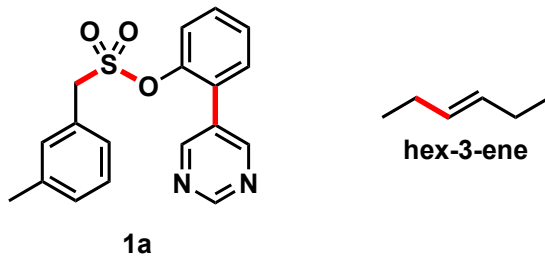
The .wfn files for NCIPILOT were generated at MN15/DGDZVP^{14,15} level of theory. Noncovalent interaction (NCI) indices calculated with NCIPILOT were visualised at gradient isosurface value of $s = 0.5$ au. These are coloured according to the sign of (λ_2) over the range of -0.1 (blue = attractive) to +0.1 (red = repulsive). All molecular structures and molecular orbitals were visualized using *Pymol* software.¹⁶ Dihedral scans were done in gas phase using MN15/def2-SVP and the energies were taken without further corrections.

Geometries of all optimized structures (in .xyz format with their associated energy in Hartrees) are included in a separate folder named *structures_xyz* with an associated README file. All these data have been deposited with this Supporting Information and uploaded to zenodo.org (DOI: 10.5281/zenodo.2775841).

All Python scripts used for data analysis have been made available - <https://github.com/bobbypaton> - under a creative commons CC-BY license.

2.9.1 Conformational considerations for starting materials

The starting materials for computational modelling, sulfonyl arene, **1a**, and *trans*-hex-3-ene, were first conformationally sampled. The possible rotamers for sulfonyl arene, **1a**, were generated by systematically varying a combination of key dihedral angles shown in red (Scheme S1) and optimising the structures. The crystal structure of *trans*-hex-3-ene was obtained as a starting point for structure optimisation; additional rotamers were generated by varying the given dihedral angle in red (Scheme S1) and doing structural optimisations. The lowest energy conformers for each starting material were used for subsequent calculations.



Scheme S1. Rotamers were generated by varying the dihedral angles in red in conformational sampling of the most stable conformer used for reaction modelling.

2.9.2 C–H activation in the presence of ligand

The amino acid ligand, *N*-Ac-norleucine, lowered the C–H activation barrier by forming a 5-membered palladacycle as shown in the main text (**ts-1'** at 20.0[‡] (20.8[‡]) kcal mol^{−1}). Other possible arrangements of this ligand were found to have higher activation barriers than **ts-1'** (Figure S13).

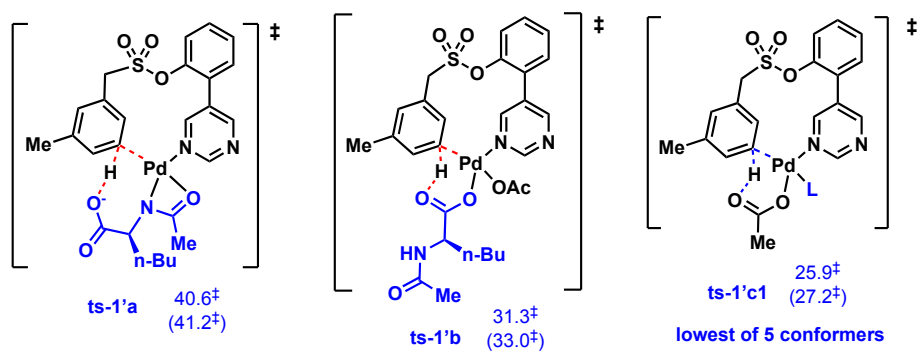


Figure S13. Possible arrangements of ligand for C–H activation step. Gibbs energies are given in kcal mol^{-1} .

2.9.3 Exact identity of the ligand in 1,2-migratory insertion TDTs

The intermediate after MPAA ligand-assisted C–H activation (**int-2'**) has the resulting ligand in imidic acid form. The subsequent 1,2-migratory insertion TS leading from here (**ts-3'a** at 41.7 kcal mol^{-1} , Figure S14) has a much higher barrier than its tautomeric form (**ts-3'b** at 27.1 kcal mol^{-1} , Figure S14). The coordination by acetate (**ts-3** at 23.2 kcal mol^{-1} , Figure S14) has the lowest barrier amongst these three possibilities. We anticipated that **ts-3** and **ts-3'b** would be rather close in energy, since they both coordinate to Pd-centre in a monodentate fashion (Figure S14), where the Pd–N interactions would dominate over other possible non-covalent interactions (NCIs) in the side chains. Although the amino acid side chain could provide better NCIs than the methyl group in acetate, it could also give rise to potentially more steric hinderance.

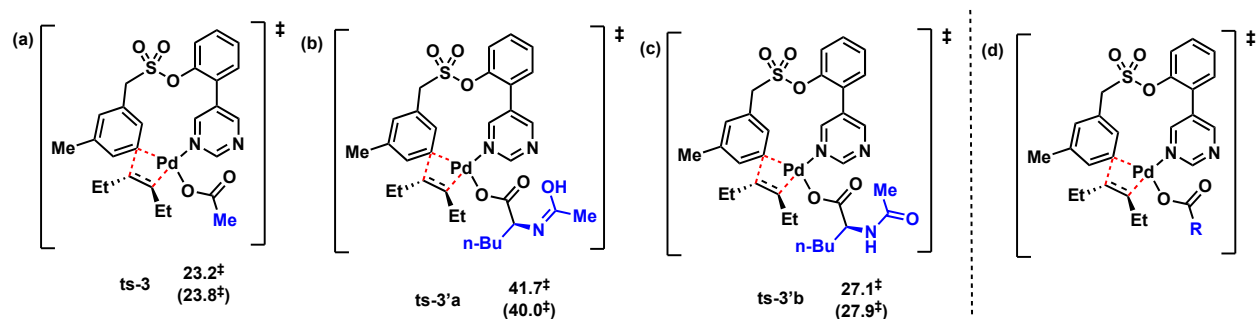


Figure S14. TDTs with either acetate (a) or amino acid in tautomeric forms (b and c) as the monodentate ligand. These can be thought of having the structure in (d) where the R-groups vary. Gibbs energies are given in kcal mol^{-1} .

In the computational study of similar systems where amino acid ligands were used for the C–H activation step, the amino acid (a.a.) was retained as a monodentate ligand for all subsequent steps.^{17,18} We envisioned that the acetate ligand and the a.a. ligand would have similar effects in 1,2-migratory insertion step and replacing the a.a. ligand with acetate would not affect the energy profile too much (Note that the main role of the a.a. ligand is in the C–H activation step). Conformational searches were thus performed for the 1,2-migratory insertion step above with either acetate or amino acid as the monodentate coordinating ligand. A total of 6 TSs were found for acetate ligand and 11 TSs for the a.a. ligand (these structures are given in folder 3_ligand_identity_in_TDTS accompanying this ESI). All these are higher than C–H activation barrier, as expected since this step was overall rate-determining and C–H activation is reversible as measured by kinetic isotopic effect experimentally. Although the lowest barrier TSs were those with the a.a. ligand, these are really close in barrier to those of the lowest TS with acetate ligand (within 2 kcal mol⁻¹). For modelling purposes, it is sufficient to use acetate instead of the full a.a. ligand since the conclusion of the mechanism will remain the same.

2.9.4 Relative stabilities of **int-5** and **int-7** and β -hydride elimination TSs

We found, via intrinsic reaction coordinates (IRC) analyses, that **int-5** eventually lead to the product formation via direct β -hydride elimination (**ts-5**, Figure 5 main text) forming a metal-bonded Pd(II) hydride, whereas **int-7** underwent acetate-assisted β -hydride elimination (**ts-7**) with much lower activation barrier. **Int-7** was much more stable than **int-5** since in the latter, the acetate group was near the 14-membered palladacycle ring, giving rise to unfavourable interactions with the arene, as shown in the NCI plot (circled in green) in Figure S15. Alternative TSs for β -hydride elimination following each of these intermediates were given in Figure S16. Note that **ts-7'**, having the Pd-coordinating acetate-O atom forming 3-membered ring in the TS is much less favoured than **ts-7**, which has the non-coordinating acetate-O atom forming 5-membered ring.

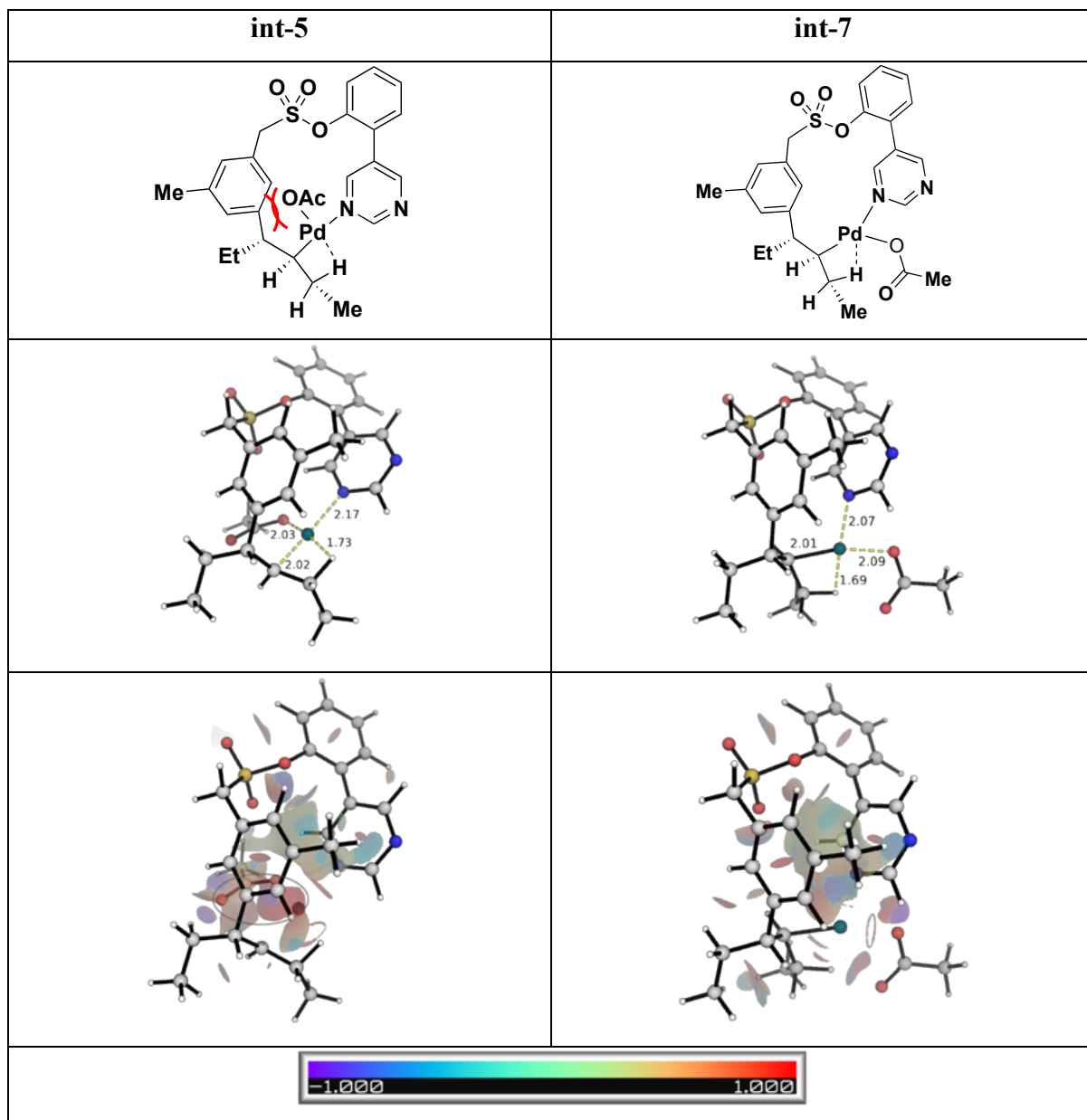


Figure S15. Relative stabilities of **int-5** and **int-7** and their NCI plots to indicate the sterics present.

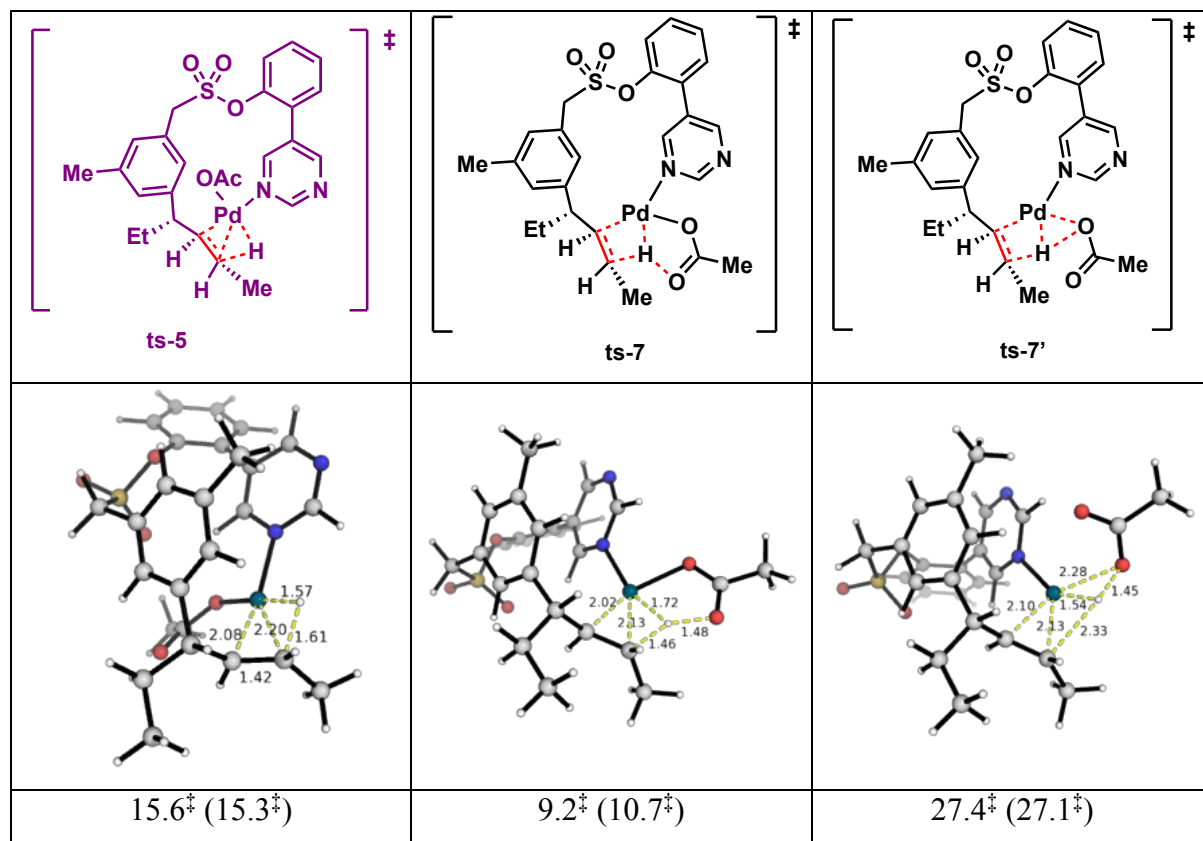
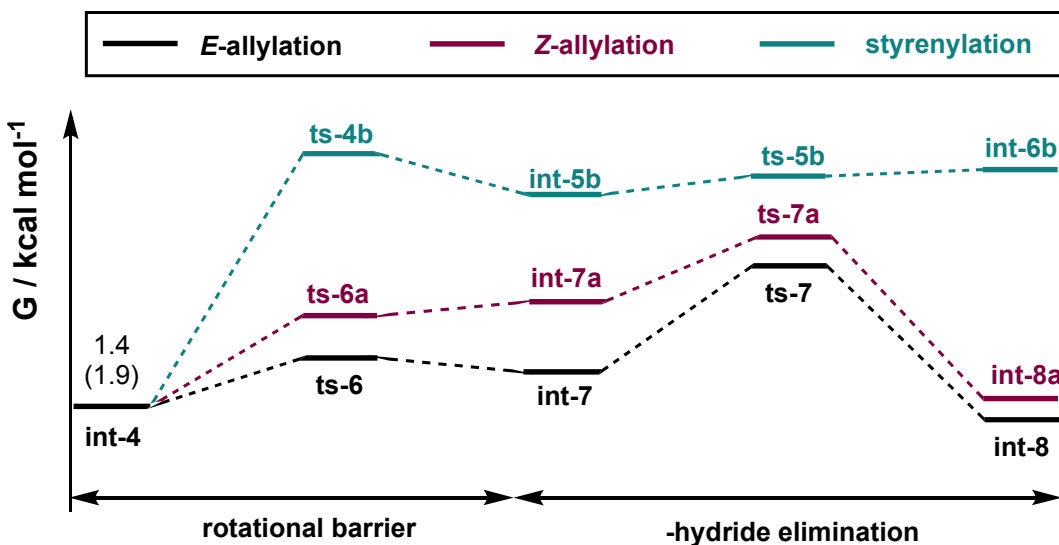


Figure S16. Alternative TSs for β -hydride elimination step to form the final product.

2.9.5 Product selectivity studies for *trans*-hexene substrate

The formations of both *E*- and *Z*-allylated products proceed via ligand-assisted β -hydride elimination whereas styrenylation proceeds via direct β -hydride elimination due to unfavourable arrangement of the acetate ligand. Styrenylation involves unfavourable palladacycle ring strain such that its direct β -hydride elimination proceeds via the displacement of the directing group pyrimidinyl-N atom by the acetate ligand that subsequently binds via bidentate mode (**ts-5b**, 19.2 kcal mol⁻¹) rather than via the intact palladacycle with the acetate ligand bound in a monodentate fashion (**ts-5b-c2**) (Figure S17). As a result, to form the styrenyl product the rotational barrier became the overall regio-determining step and this required a very high barrier as the palladacycle experienced huge strain when H_s was brought to interact agostically with Pd(II) centre (Figure S18(ii)).



Reaction product	direct β -H elimination				ligand-promoted β -H elimination				Overall barrier ^a
	ts-4x	int-5x	ts-5x	int-6x	ts-6x	int-7x	ts-7x	int-8x	
<i>E</i> -allyl (x=nil)	15.0 [‡] (14.9 [‡])	12.4 (12.7)	15.6 [‡] (15.3 [‡])	8.5 (8.4)	4.3 [‡] (4.7 [‡])	3.8 (6.0)	9.2 [‡] (10.7 [‡])	-0.4 (-0.3)	7.8 (8.8)
<i>Z</i> -allyl (x=a)	16.8 [‡] (16.5 [‡])	14.7 (15.1)	17.6 [‡] (17.6 [‡])	9.6 (10.0)	5.9 [‡] (6.4 [‡])	7.0 (8.9)	11.3 [‡] (12.7 [‡])	0.7 (0.6)	9.9 (10.8)
styrenyl (x=b)	21.0^{‡, b} (21.8[‡])	17.9 (18.7)	19.2 ^{‡, c} (19.2 [‡])	20.4 (18.3)	21.0^{‡, b} (21.8[‡])	3.9 (4.7)	48.5 [‡] (48.3 [‡])	10.5 (8.3)	19.6 (19.9)

^a We take the lowest value of the two. Both *E*- and *Z*-allylation preferred acetate-promoted β -hydride elimination, whereas styrenylation preferred direct β -hydride elimination via Pd(II)-hydride complex.

^b Rotational TS for styrenylation are the same regardless of whether β -hydride elimination occurs directly or via ligand involvement. The prerequisite is to bring the H_s atom to interact agostically with Pd(II)-centre.

^c The TS where the directing group got displaced (ts-5b) has a lower activation barrier than the one where it remains coordinated (ts-5b-c2) since the former released the unfavourable strain in the palladacycle.

Table S10. Gibbs energies for selectivity studies for *trans*-hexene. TDTs values are given in bold.

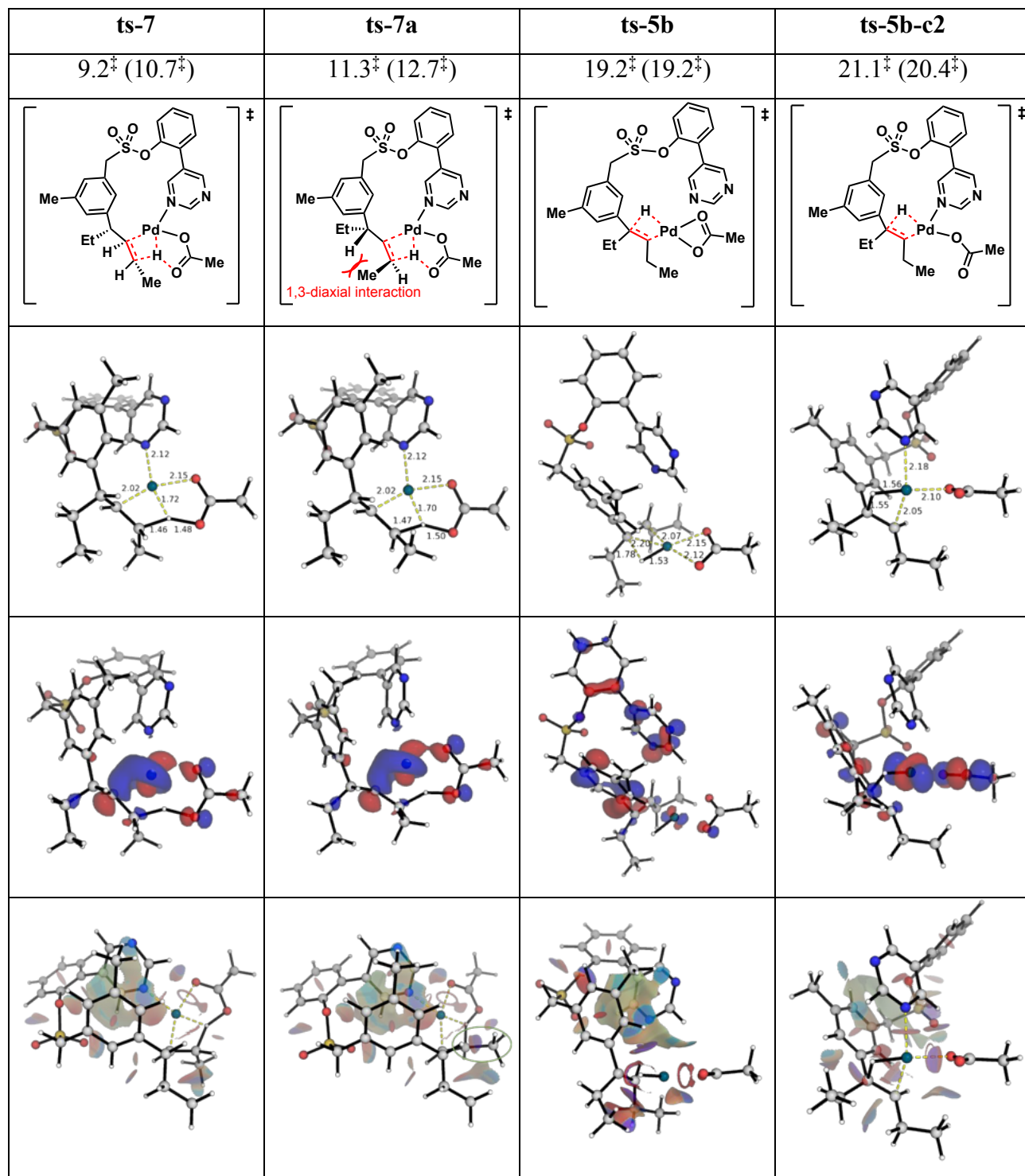


Figure S17. Product selectivity studies. The β -hydride elimination TSs for each product formation is given, with their HOMOs (isosurface value of 0.05) and NCI plots.

The dihedral angle scans allow us to compare the rotational barriers required to form allyl- vs styrenyl-product since the rotational barrier for the latter is regio-determining. We can see that styrenylation has a hugely disfavoured ring strain when the required H atom (H_s in Figure S18(ii)) is brought to interact agostically with Pd(II) centre – a prerequisite for the subsequent β -hydride elimination. Note that as discussed in the main text, the allylation involved steps that did not impose any strain on the 14-m palladacycle whereas the styrenylation severely distorted the palladacycle giving rise to hugely unfavourable ring strains.

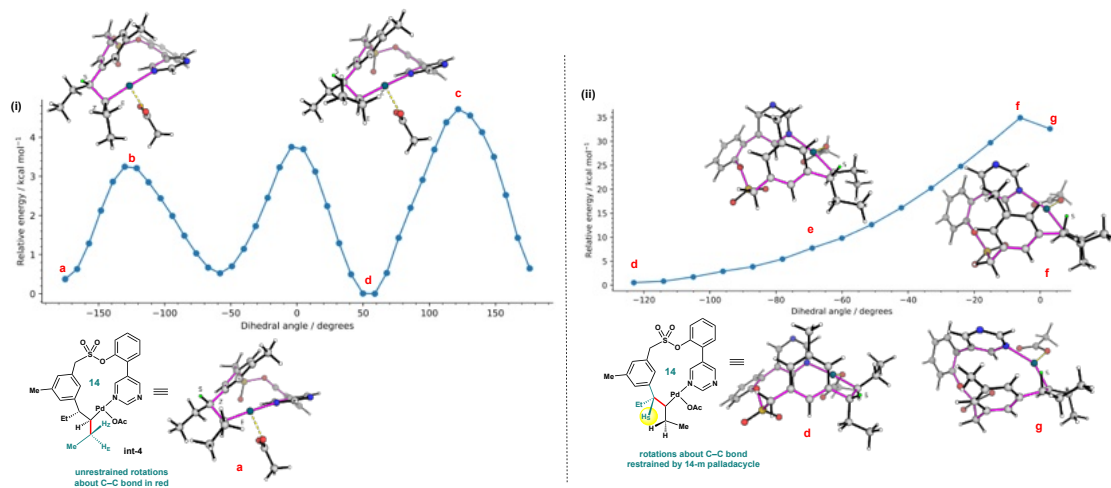
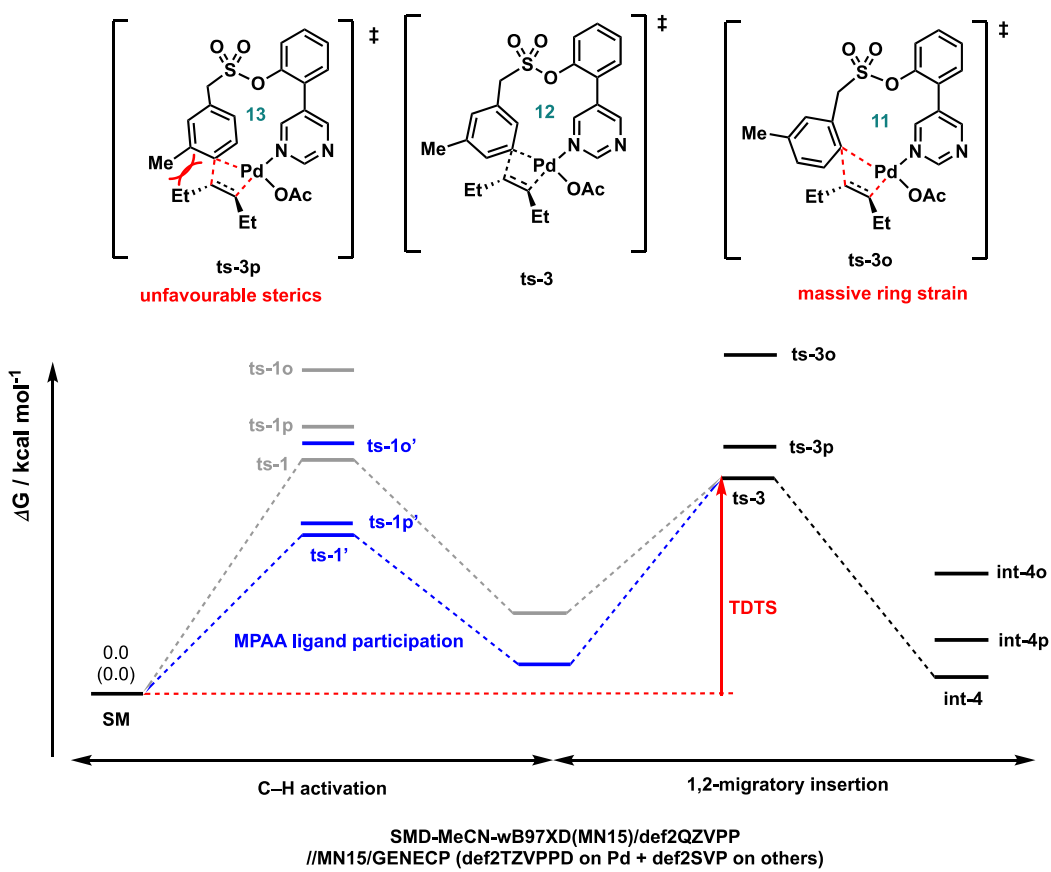


Figure S18. Dihedral angle scan (about C–C bond in red) for rotational barrier for the formation of (i) *E*-/*Z*-allylated products and (ii) styrenyl product for *trans*-hexene substrate. Note the different energy scales used. In (ii), note the position of styrenyl proton (H_s , labelled *S* in green), which is restrained in a position away from Pd(II)-centre by the conformationally rigid ring (outlined in purple).

2.9.6 Arene site-selectivity (HOMO, NCI plots and isodesmic studies)

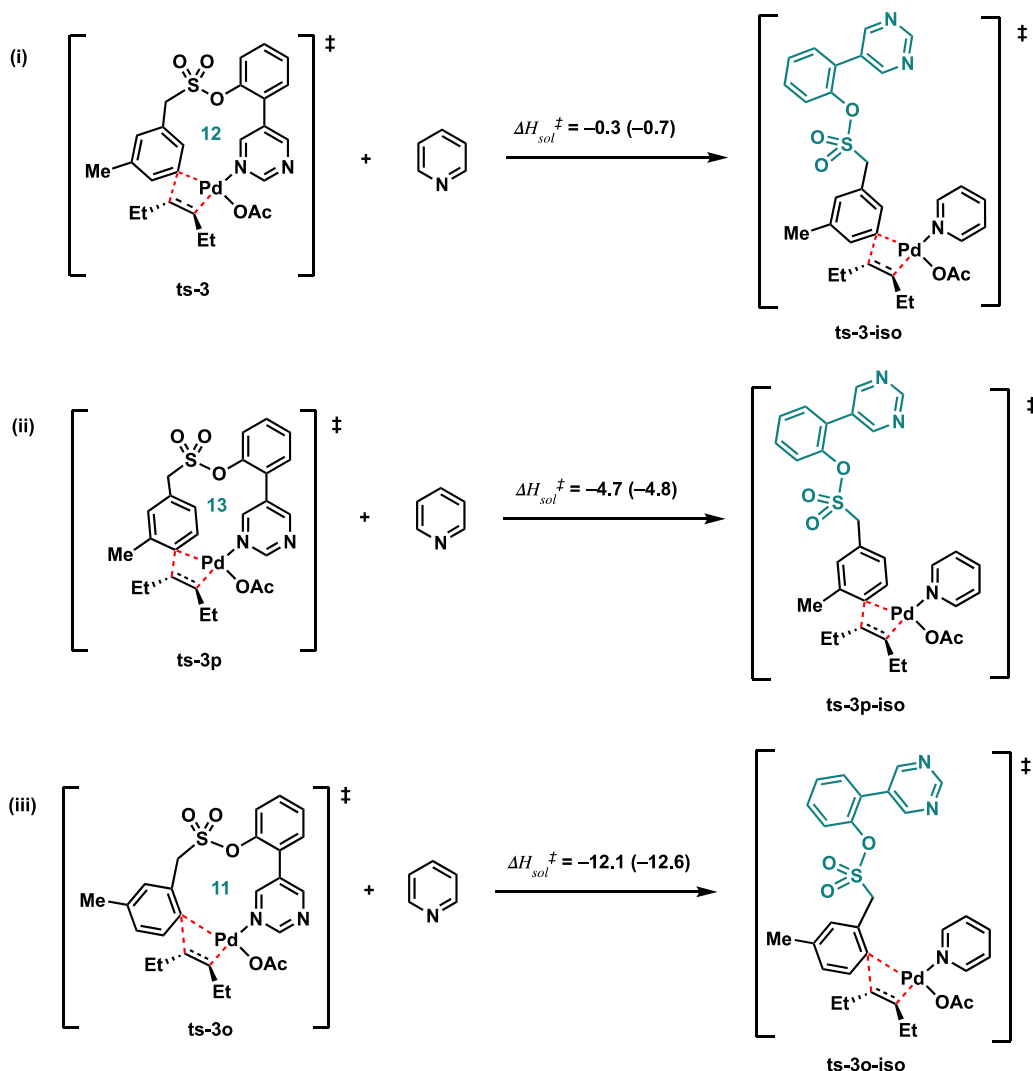
The *ortho*-/*para*-positions on the arene for potential activation were compared to *meta*-activation. The C–H activation and 1,2-migratory insertion steps were studied. The comparative energies for the key steps were given in Table S11. For the turnover frequency determining step, *para*-insertion (**ts-3p**) was 3.9 kcal mol⁻¹ higher in activation barrier than *meta*-insertion (**ts-3**), translating to 1 in 222 selectivity; *ortho*-insertion (**ts-3o**) was 12.7 kcal mol⁻¹ higher than ts-3, making *ortho*-insertion uncompetitive (1 in 40 million). These agreed well with observed selectivities which can be traced to unfavorable sterics involved in *ortho*- and *para*-addition (Figure S19).



Allylation site	ts-1x	ts-1x'	ts-3x	int-4x
<i>meta-</i> (x=nil)	26.7 [‡] (28.2 [‡])	20.0 [‡] (20.8 [‡])	23.2[‡] (23.8[‡])	1.4 (1.9)
<i>ortho-</i> (x=o)	35.8 [‡] (34.9 [‡])	28.7 [‡] (29.2 [‡])	37.0[‡] (35.5[‡])	19.2 (18.2)
<i>para-</i> (x=p)	28.6 [‡] (28.6 [‡])	20.5 [‡] (20.0 [‡])	28.2[‡] (26.7[‡])	8.4 (8.2)

Table S11| Arene site-selectivity studies. MPAA ligands lowered C–H activation in all cases such that 1,2- migratory insertion (ts-3x) becomes the TDTS whose barriers are given in bold.

In addition to the stereoelectronic effects associated with arene site selectivity, the ring strain energies in these TSs were calculated from the reaction enthalpy of the isodesmic reaction^{19,20} shown in Scheme S2. Specifically, a hypothetical pyridine ligand was used for TS searches to release the ring strain where the directing group (DG) got uncoordinated. The starting conformation for the DG (highlighted in green, Scheme S2) in all 3 cases was made the same in a linear form for subsequent TS searches. The enthalpies of the reactions were further corrected with SMD solvation model: $\Delta H_{sol}^{\ddagger} = \Delta H_{gas}^{\ddagger} - \Delta E_{gas}^{\ddagger} + \Delta E_{sol}^{\ddagger}$. The calculations showed that the *meta*-insertion TDTS had the lowest ring strain at 0.3 kcal mol⁻¹, followed by *para*-insertion TDTS, with 4.7 kcal mol⁻¹; *ortho*-insertion TDTS had the largest ring strain at 12.1 kcal mol⁻¹. These values are in excellent quantitative agreement with the selectivity studies (Table S11, where *para*-TDTS is about 4 kcal mol⁻¹ and *ortho*-TDTS is about 12 kcal mol⁻¹ higher than *meta*-TDTS).



Scheme S2. Computed ring strain energies by study of isodesmic reaction where a hypothetical pyridine ligand is involved. Enthalpies quoted are corrected with solvent effect and in kcal mol^{-1} .

The HOMOs for insertion TDTSSs for *meta-/ortho-/para*-activation were plotted in Figure S19 Top. These show similar electron distributions, suggesting that electronic factors are less important in the selectivity of arene site activation. NCI plots (Figure S19 Bottom) show that **ts-3p** was sterically disfavoured when the methyl-group on the ring came close to the alkene being added whereas in **ts-3o**, the excessive ring strain made this TS highly strained (the directing group got twisted out of shape), giving rise to unfavourably high activation barrier. The possibility of addition to the other *ortho*-site would bring the methyl-group into close proximity of the alkene being added, further increasing the activation strain and was thus not considered.

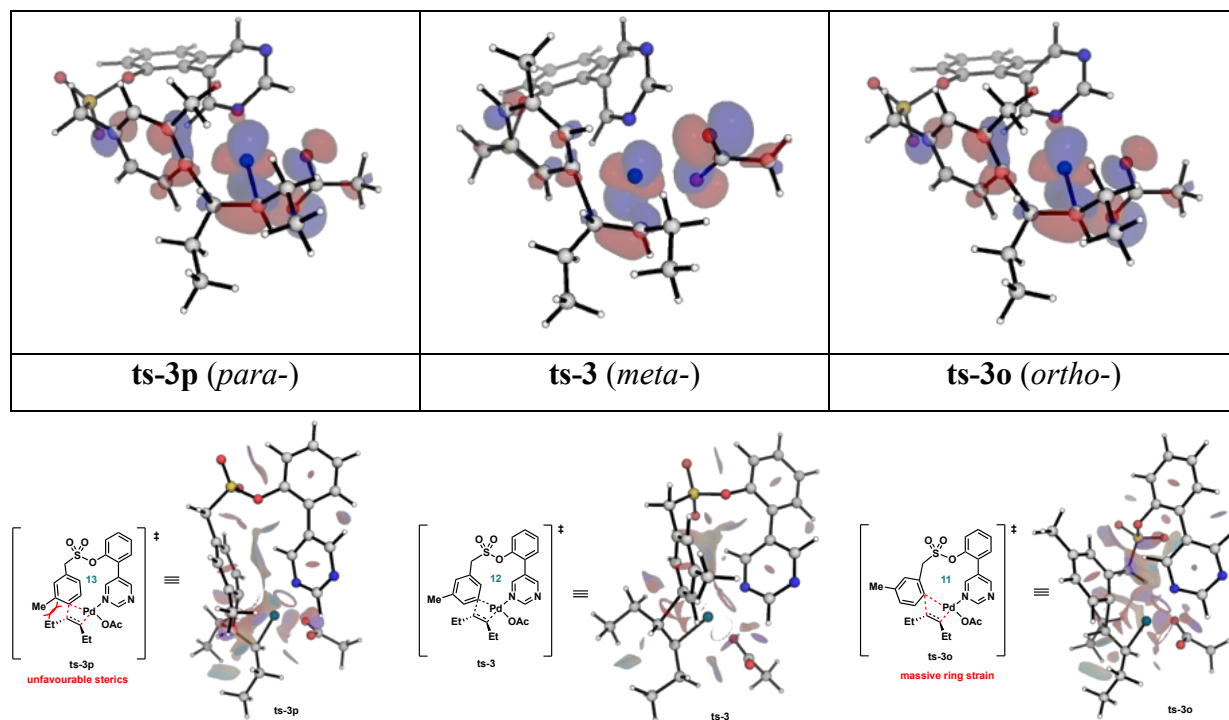
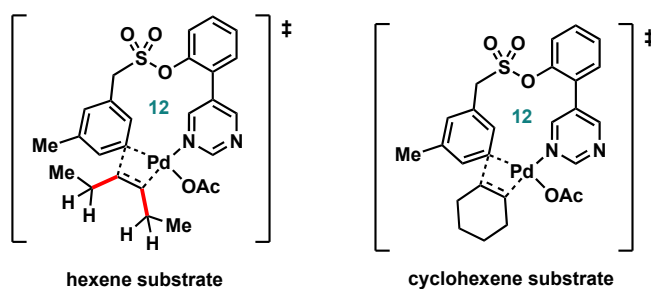


Figure S19. Insertion TSs from *para*-, *meta*- and *ortho*-activated complexes. Top: HOMOs at an isovalue of 0.04. Bottom: NCI plots.

2.9.7 General conformational sampling of TDTSSs (1,2-migratory insertion step)

Once a TS was found, the structure was used as starting guesses for searching TS conformers. The palladacycle ring was frozen and rotamers along C–C bonds in red (Scheme S3) were generated for TS conformational searches. Altogether, 9 TSs were found for each orientation of alkene (18 TSs for each of *trans*-hexene and *cis*-hexene) and 4 TSs were found for each orientation of cyclohexene (8 TSs altogether). The optimized TS structures and their relative energy barriers with respect to the lowest barrier TS for *trans*-hexene substrate ($\Delta\Delta G^\ddagger$) were shown in Figure S20.



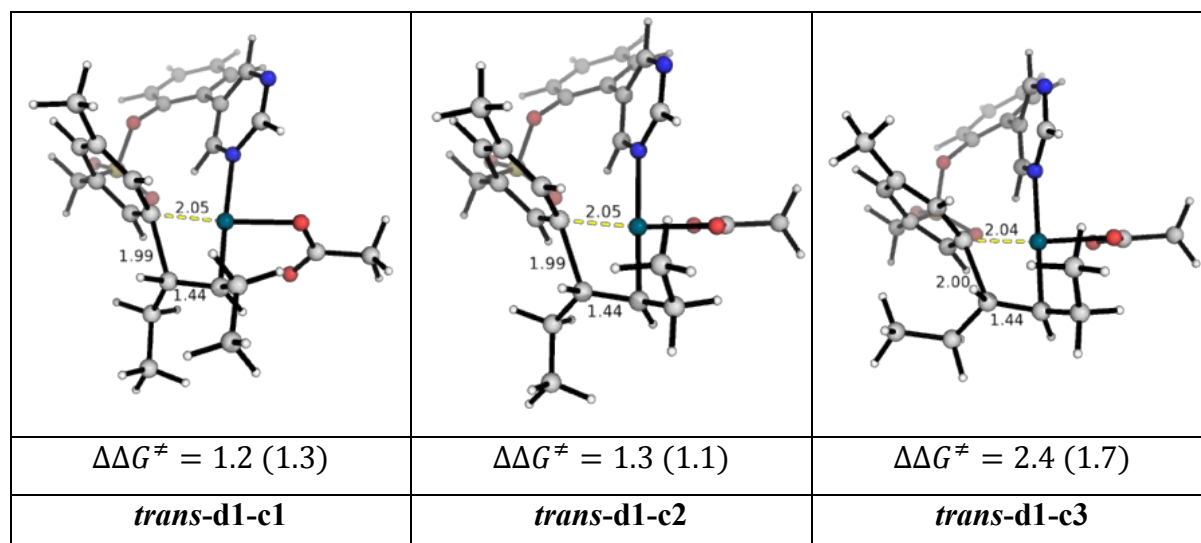
Scheme S4. Rotamers were generated by varying the dihedral angles in red in conformational sampling of the 1,2-migratory insertion TDTSSs for *trans*- and *cis*-hexene substrates; for cyclohexene substrate, the buckling of the half-chair in different orientations were considered.

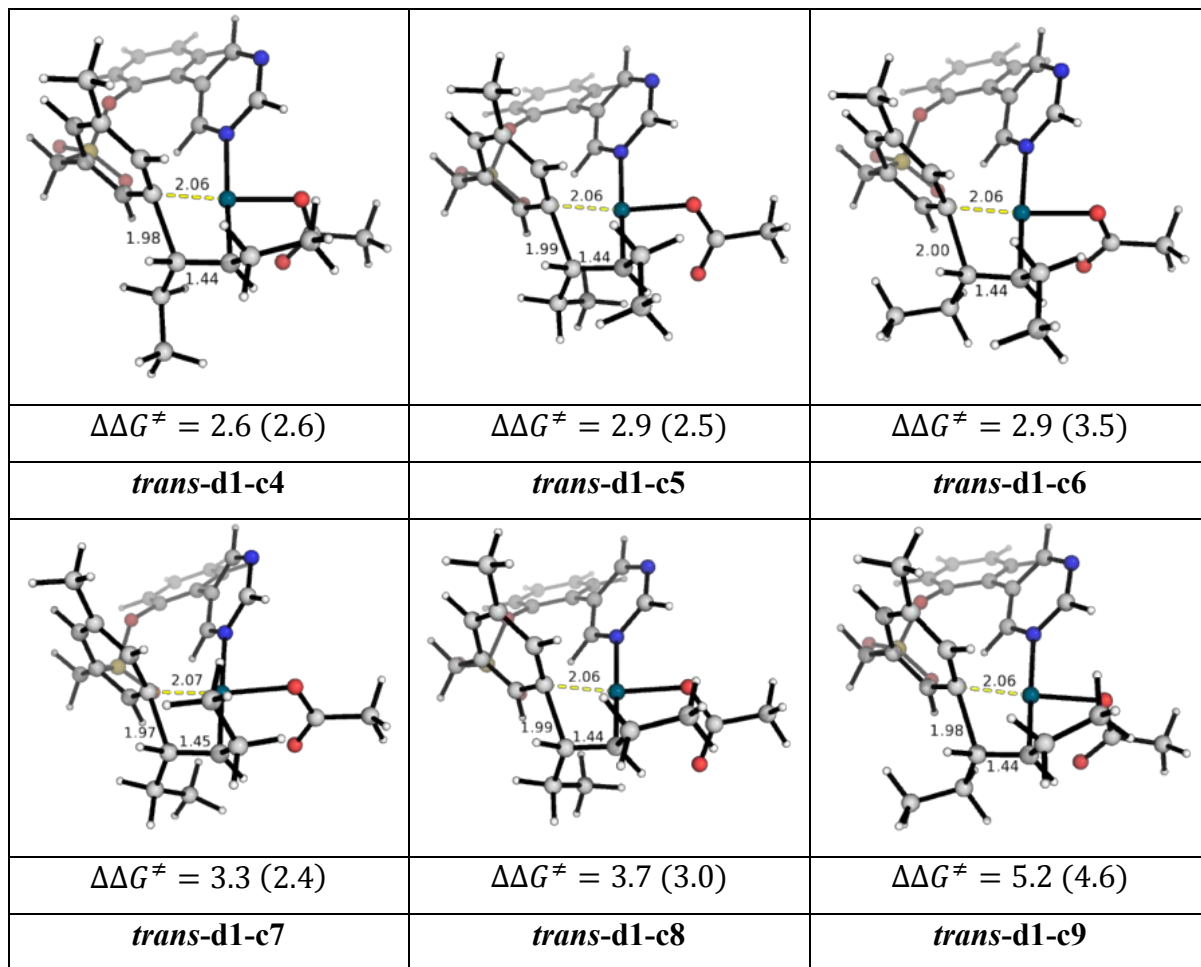
Boltzmann weighting and selectivity

All TDTS conformers were used for Boltzmann weighting to give selectivity ratio. Standard procedures for Boltzmann weighting were applied (see, for example, Equation (2) of ref.²¹ and SI of ref.²²); specifically, the selectivity between two products A and B were calculated *via*

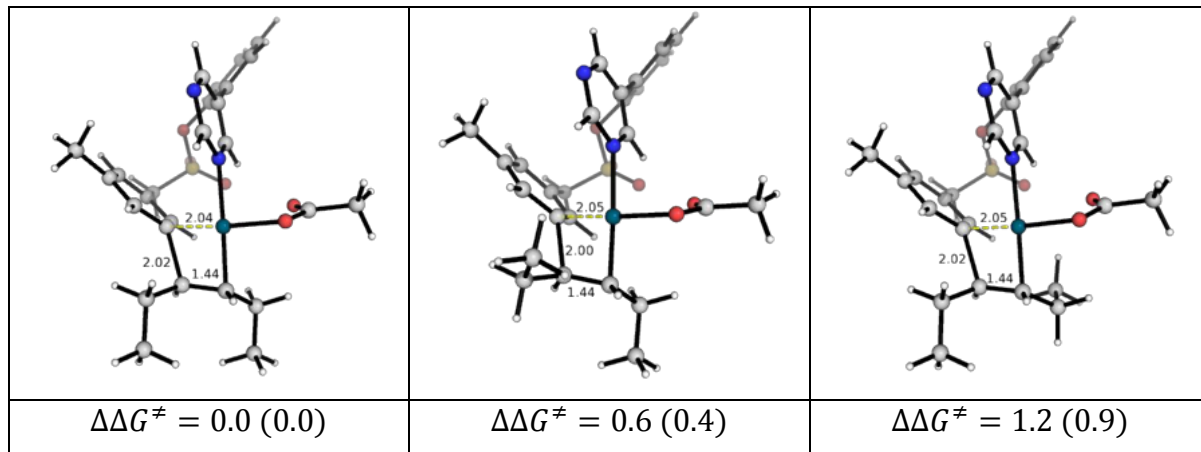
$$\frac{[A]}{[B]} = \frac{\sum_{i \in \text{all confs}, A}^N e^{-\Delta\Delta G_{0i,A}^\ddagger / RT}}{\sum_{j \in \text{all confs}, B}^N e^{-\Delta\Delta G_{0j,B}^\ddagger / RT}} \quad (1)$$

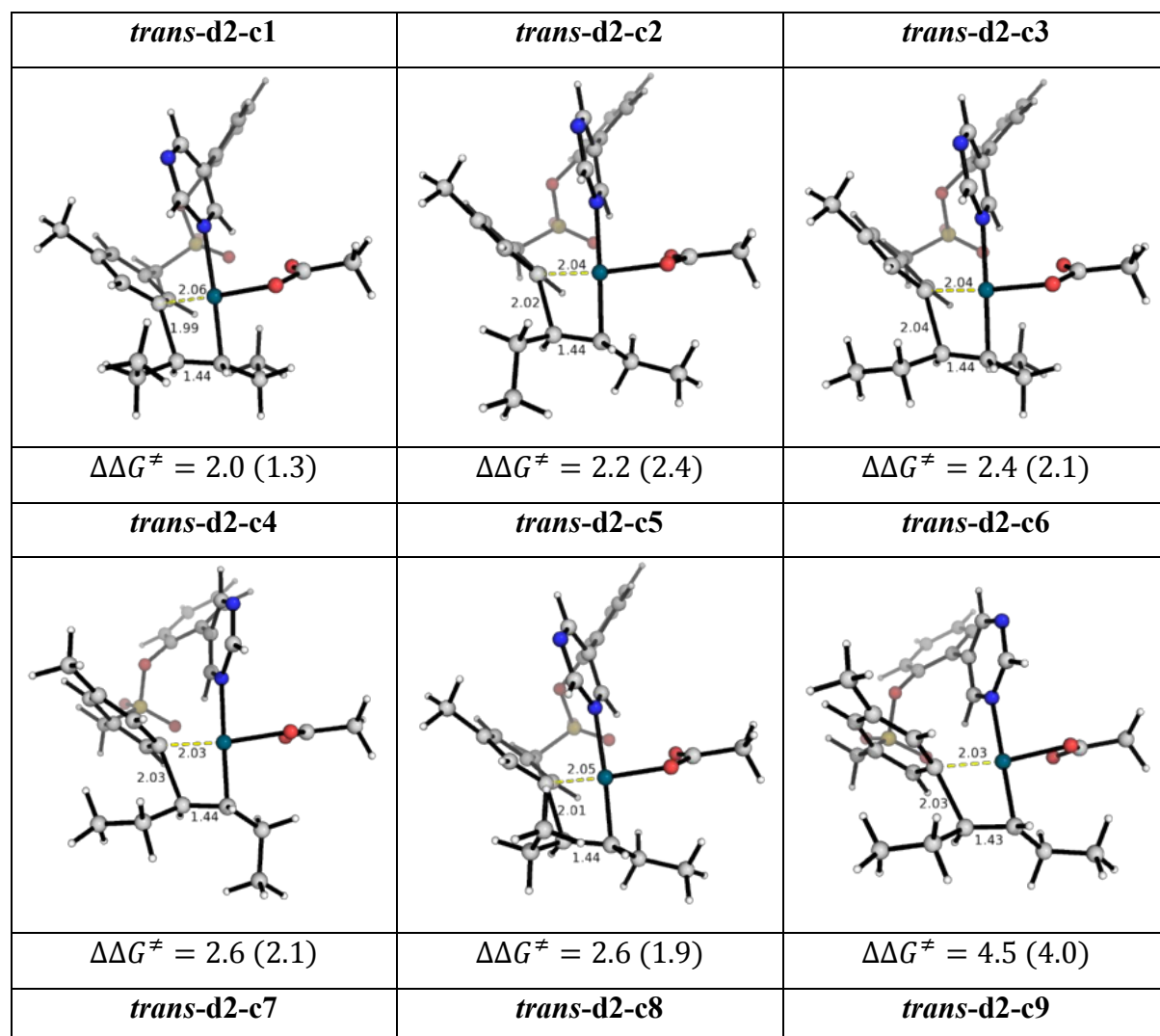
where $\Delta\Delta G_{0i,X}^\ddagger = \Delta G_{i,X}^\ddagger - \Delta G_{0,X}^\ddagger$ is the energy difference between the i^{th} conformer of product X ($X = A, B$) and the lowest energy conformer of all products, state 0.



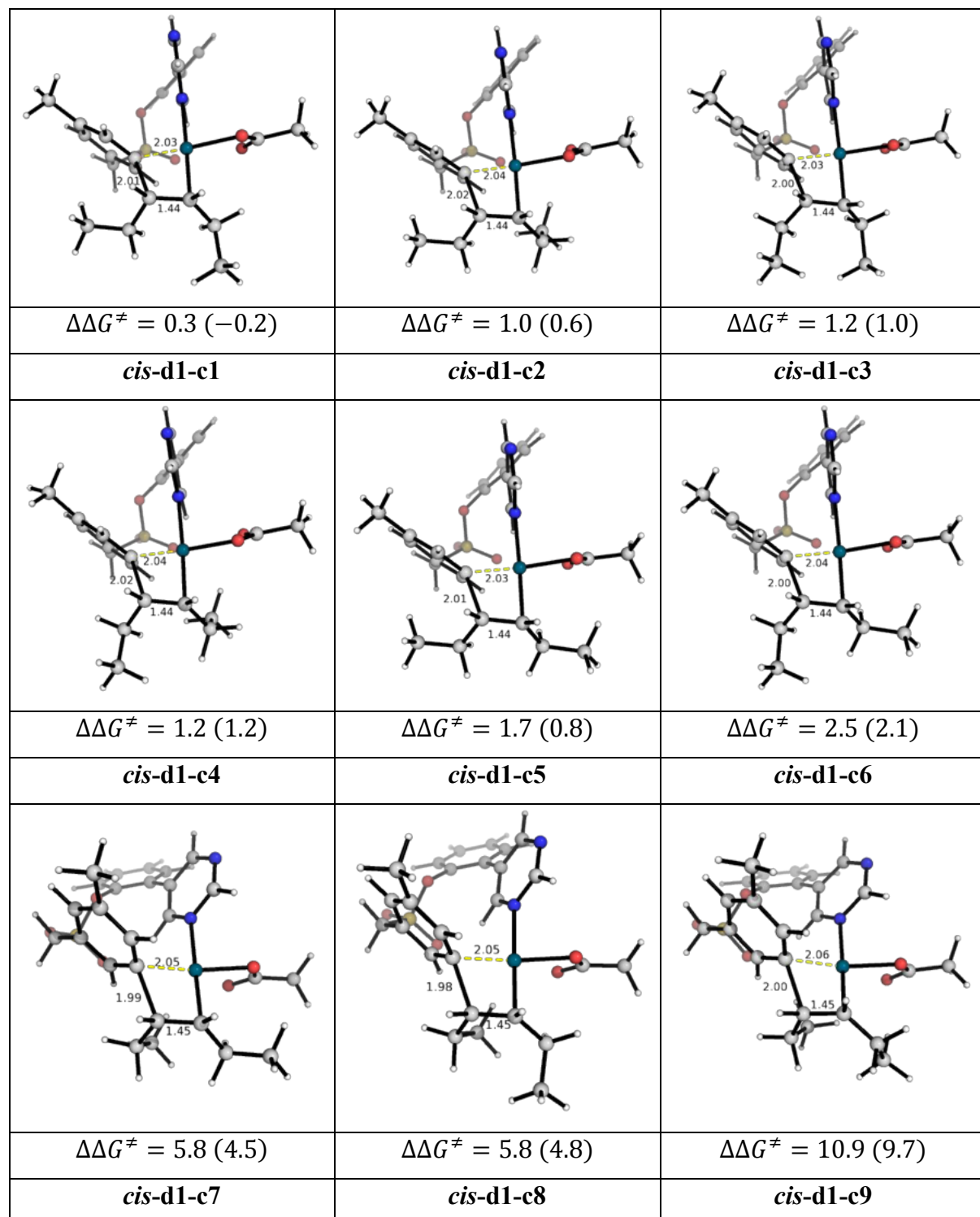


(a) Conformers for 1,2-migratory insertion TDTs for diastereomer 1 (d1) formation from *trans*-hexene.

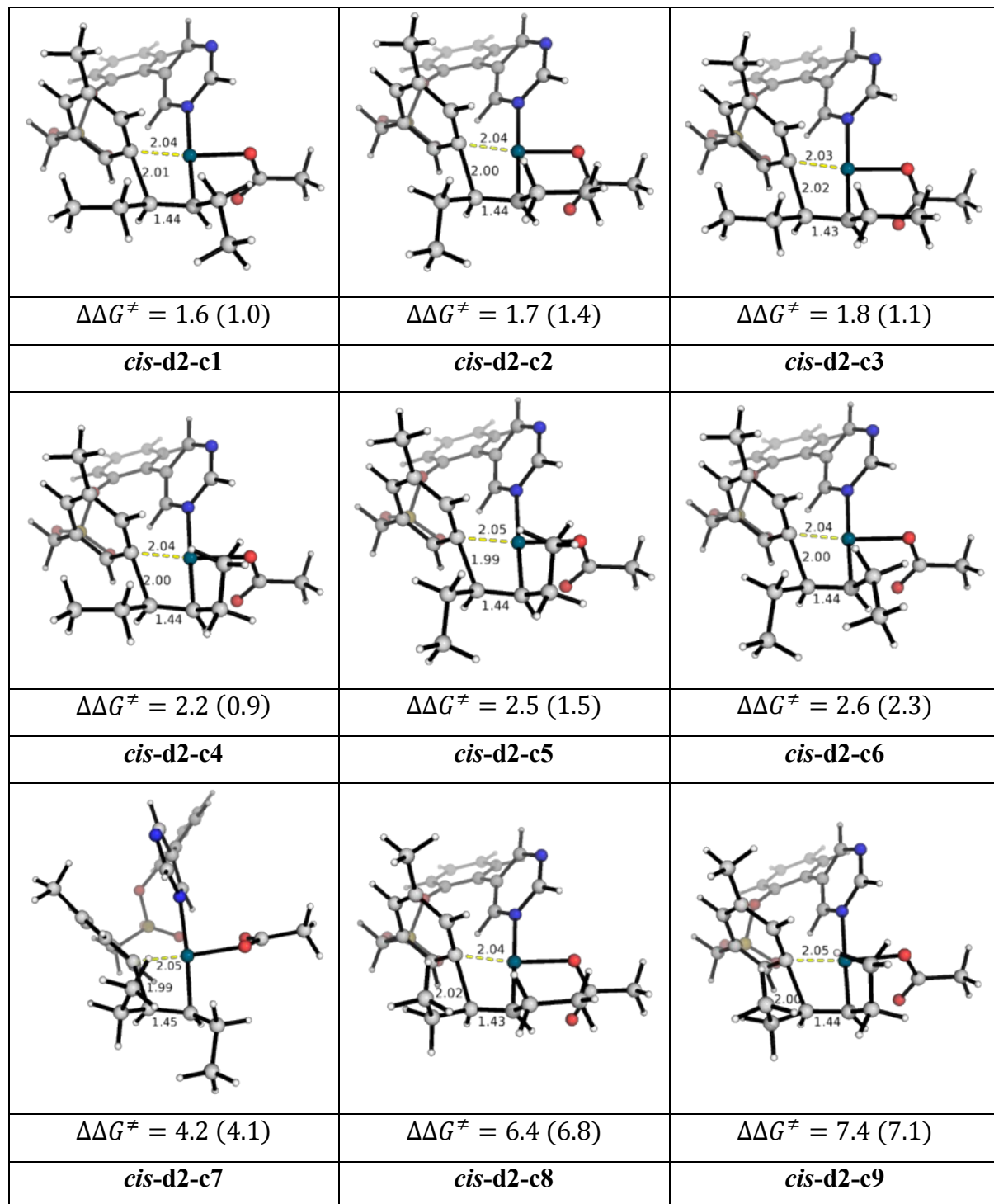




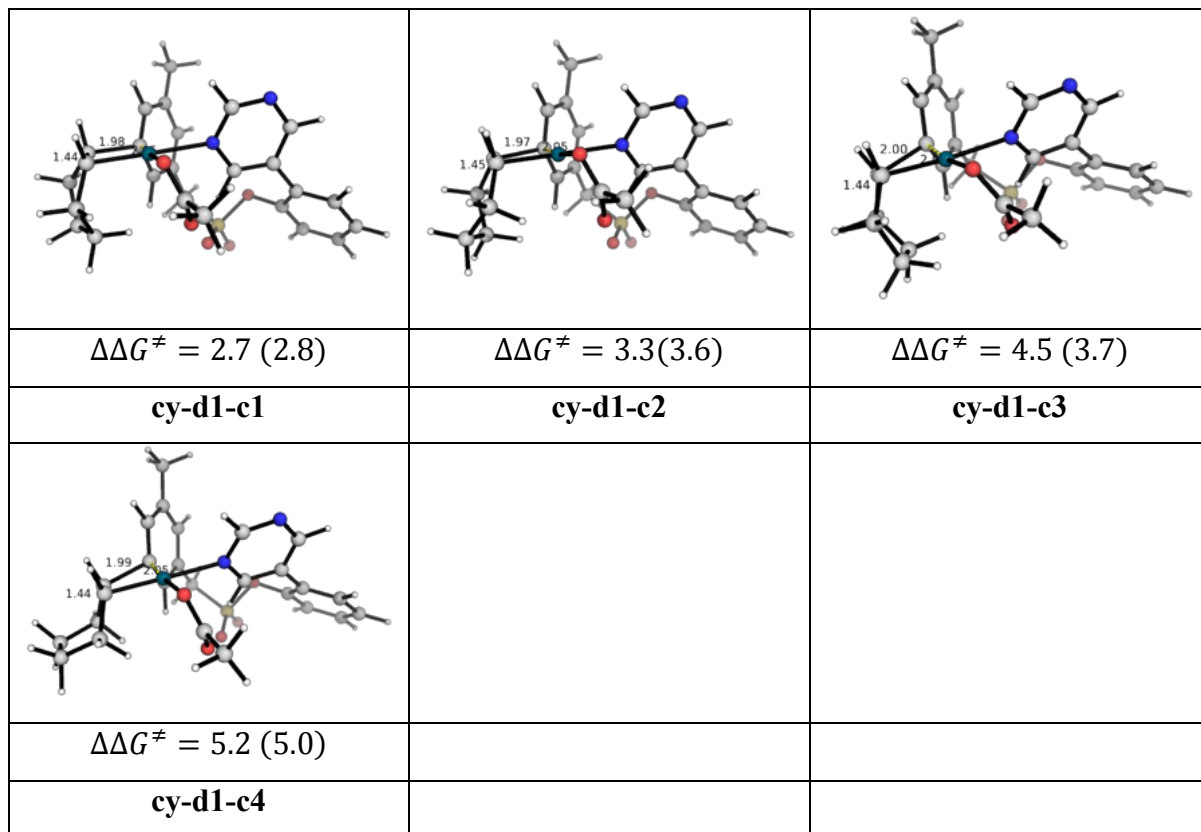
(b) Conformers for 1,2-migratory insertion TDTs for diastereomer 2 (d2) formation from *trans*-hexene.



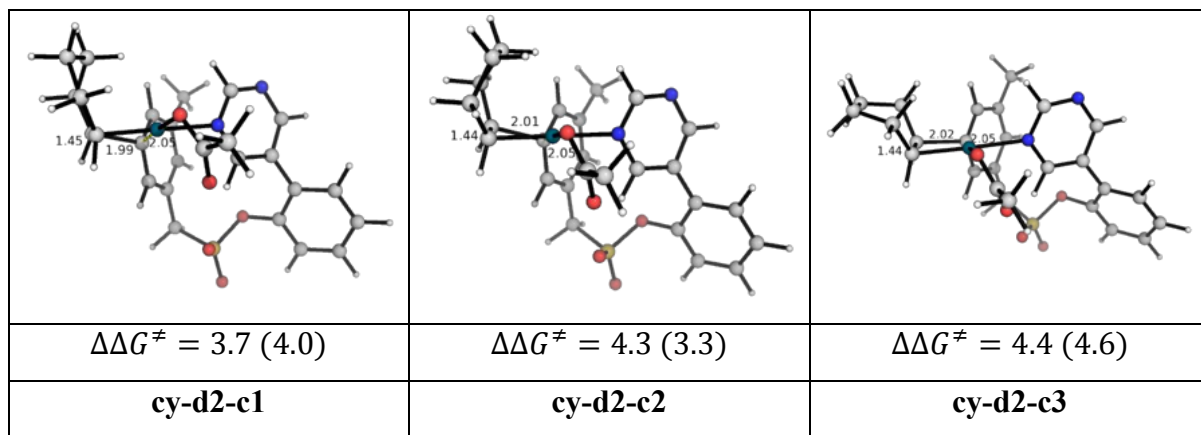
(c) Conformers for 1,2-migratory insertion TDTs for diastereomer 1 (d1) formation from *cis*-hexene.



(d) Conformers for 1,2-migratory insertion TDTs for diastereomer 2 (d2) formation from *cis*-hexene.



(e) Conformers for 1,2-migratory insertion TDTs for diastereomer 1 (d1) formation from cyclohexene (cy).



$\Delta\Delta G^\ddagger = 4.4 \text{ (4.8)}$		
cy-d2-c4		

(f) Conformers for 1,2-migratory insertion TDTs for diastereomer 2 (d2) formation from cyclohexene (cy).

Figure S20. Optimized TS geometries for 1,2-migratory insertion TDTs step for *trans*-hexne (a and b), *cis*-hexene (c and d) and cyclohexene (e and f). All TSs were taken relative to the same minima (*trans*-d2-c1). Relative $\Delta\Delta G^\ddagger$ values are in kcal mol⁻¹. Bond lengths are given in Angstroms.

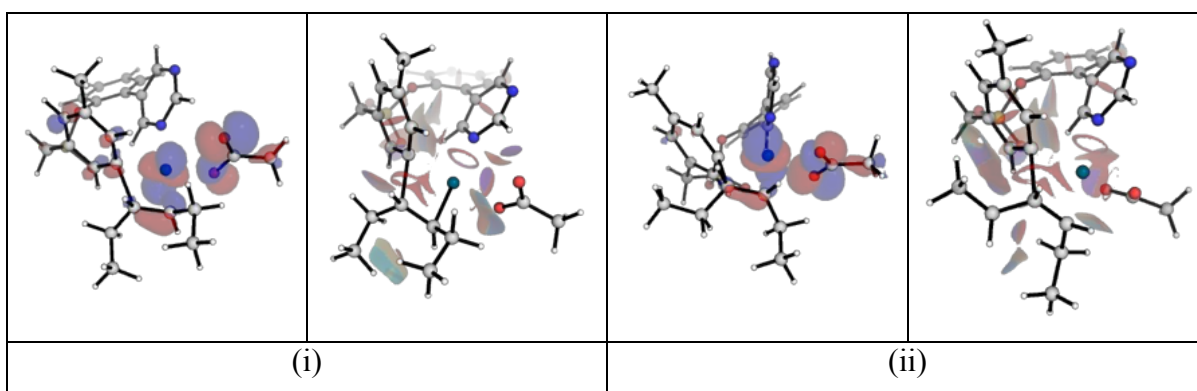
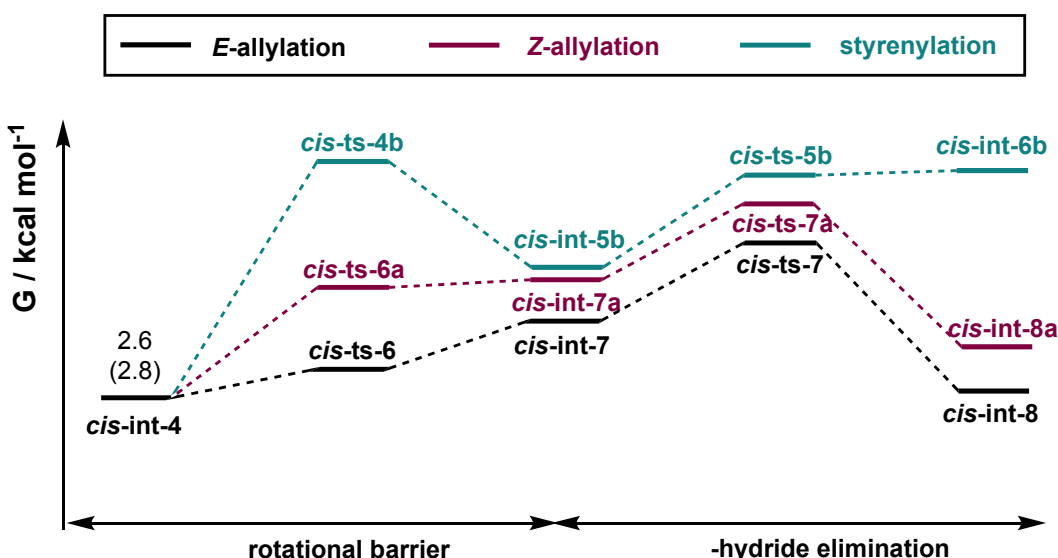


Figure S21. HOMO (isosurface value of 0.04) and NCI plots for the 1,2-migratory insertion TDTs lowest barrier conformer for (i) *trans*-hexene and (ii) *cis*-hexene. The comparisons show that stereoelectronics are rather similar, suggesting similar reactivities.

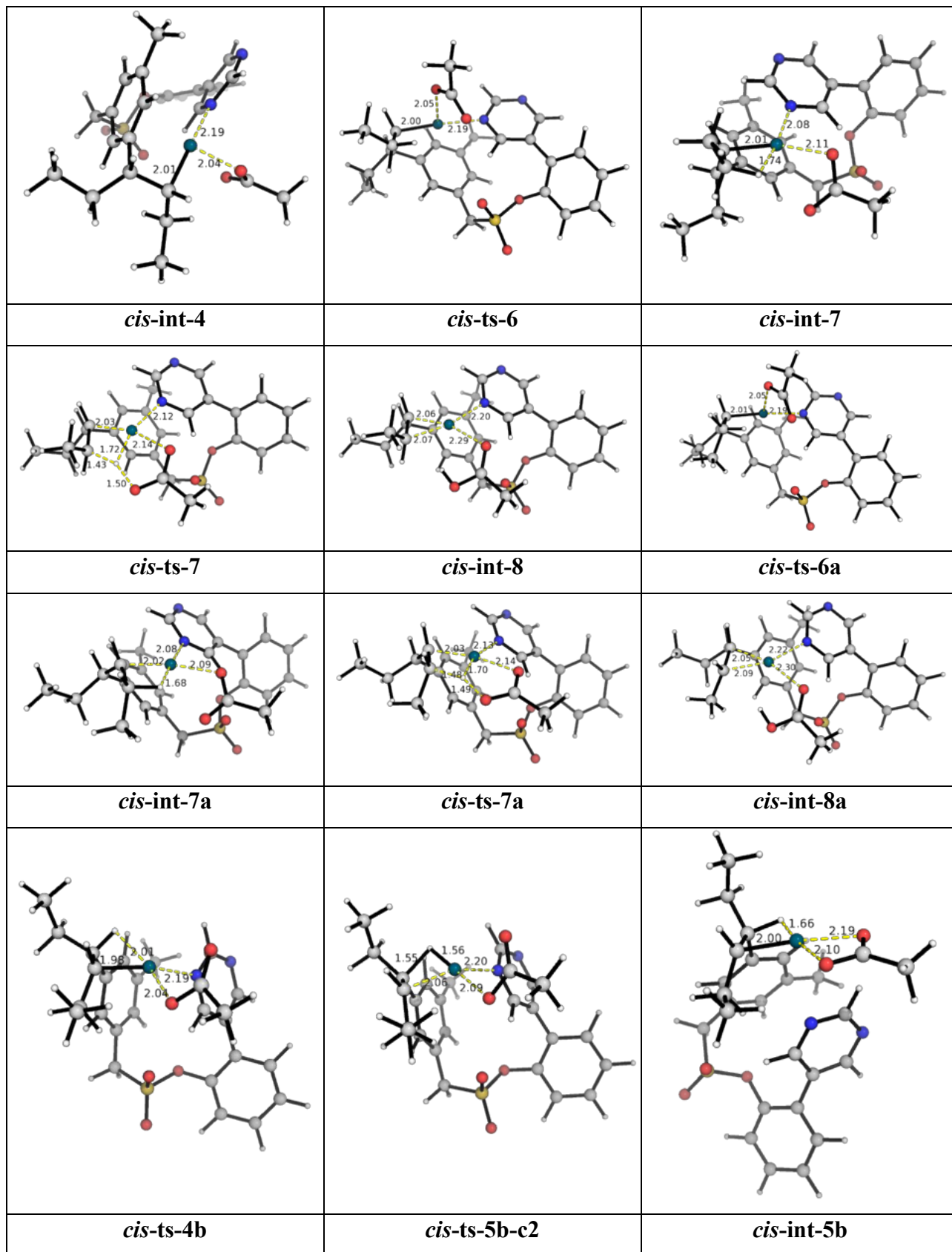
2.9.8 Product selectivity studies for *cis*-hexene substrate

Following from results using *trans*-hexene (section 2.9.5), the lowest pathways for *cis*-hexene product selectivity were studied and the key TS structures shown. Here again, for styrenylation, the TS where the DG got displaced (*cis*-ts-5b at 16.1^\ddagger (15.3^\ddagger) kcal mol $^{-1}$) has a lower activation barrier than the one where it remained coordinated (*cis*-ts-5b-c2 at 23.1^\ddagger (22.5^\ddagger) kcal mol $^{-1}$) since the former released the unfavourable strain in the palladacycle (Figure S22).



Reaction product	direct β -H elimination				ligand-promoted β -H elimination				Overall barrier
	<i>cis</i> -ts-4x	<i>cis</i> -int-5x	<i>cis</i> -ts-5x	<i>cis</i> -int-6x	<i>cis</i> -ts-6x	<i>cis</i> -int-7x	<i>cis</i> -ts-7x	<i>cis</i> -int-8x	
<i>E</i> -allyl (x=nil)	—	—	—	—	4.9^\ddagger (5.1^\ddagger)	10.8 (10.5)	13.8[‡] (14.9[‡])	3.5 (3.0)	11.2 (12.1)
<i>Z</i> -allyl (x=a)	—	—	—	—	10.7^\ddagger (11.4^\ddagger)	11.7 (13.3)	17.4[‡] (18.6[‡])	7.1 (6.4)	14.8 (15.8)
styrenyl (x=b)	20.8[‡] (22.2[‡])	11.7 (12.3)	16.1^\ddagger (15.3^\ddagger)	17.1 (14.8)	—	—	—	—	18.2 (19.4)

Table S11. Gibbs energies for selectivity studies for *cis*-hexene. TDTs values are given in bold.



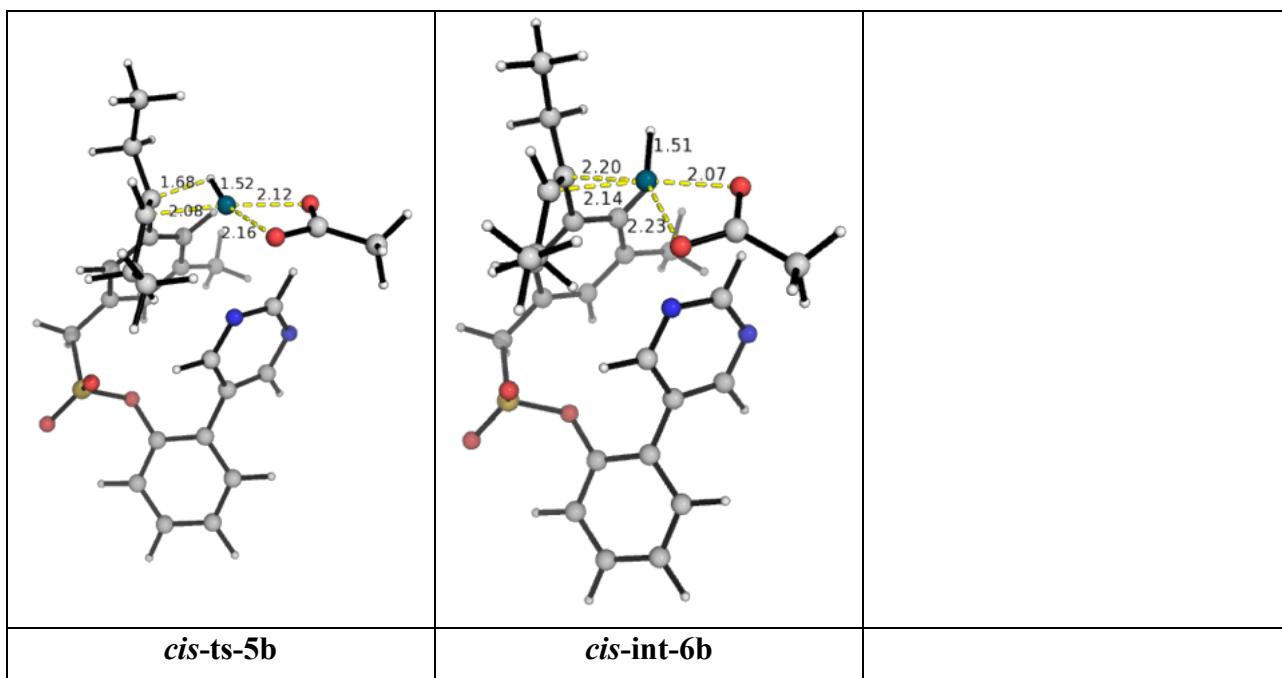


Figure S22. Optimised TS structures for selectivity studies using *cis*-hexene substrate.

HOMOs for ligand-assisted β -H elimination for both allylation using *cis*-hexene substrate (Figure S23) are similar to each other and similar to those for *trans*-hexene (Figure S17), where a σ^*_{CC} bond is broken and a π_{CC} bond is formed as the deprotonation occurred. The differences in the *E*-/*Z*-allylation stereoselectivity could arise due to the slightly less favourable NCIs in *Z*-allylation (Figure S23).

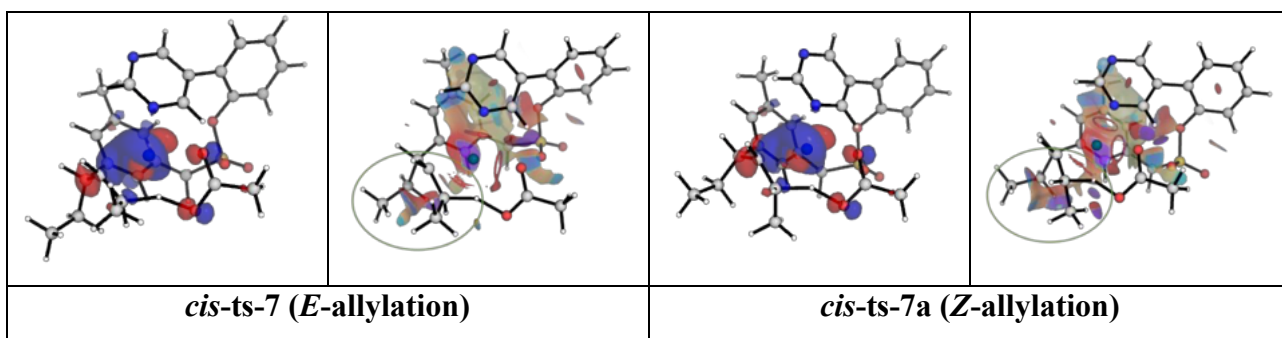


Figure S23. HOMOs (isosurface value 0.05) and NCI plots for *E*- vs *Z*-allylated product selectivity for *cis*-hexene substrate.

Although for allylation, the ligand-assisted β -H elimination is the r.d.s. for product selectivity, the rotational barrier to bring the H_s atom to interact agostically with Pd(II) centre before direct β -H elimination is the r.d.s. for styrenylation. A comparison between such rotations by the dihedral angle scans along key C–C bonds can be instructive (Figure S24).

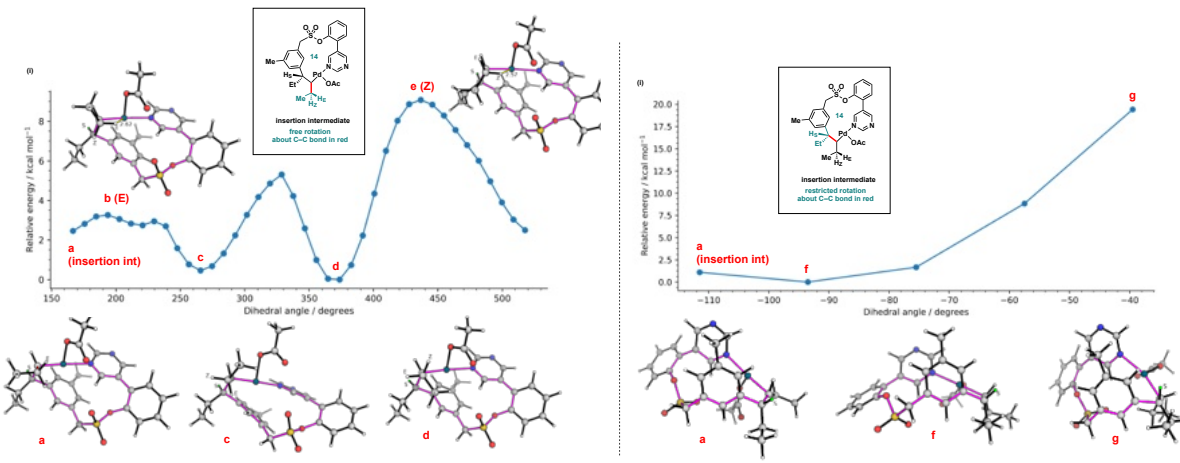


Figure S24. Dihedral angle scan (about C–C bond in red) for rotational barrier for the formation of (i) *E*-/*Z*-allylated products and (ii) styrenyl product for *cis*-hexene substrate. Note the different energy scales used. In (ii), the position of styrenyl proton (H_s , labelled *S* in green) is restrained away from Pd(II)-centre by the conformationally rigid ring (outlined in purple).

2.9.9 Product selectivity studies for cyclohexene substrate

Initial dihedral angle scans were performed about the key C–C bonds to locate rotational barriers bringing the H atom (for subsequent β -H elimination) to interact agostically with Pd(II)-centre (Figure S25). Only rotational barriers for *Z*-allylation could be located; both *E*-allylation and styrenylation had rotational barriers that were about 30 kcal mol⁻¹ higher than for *Z*-allylation; these arise due to unfavourable ring distortions imposed by the rigid cyclohexyl ring fused to the rigid palladacycle in the insertion intermediate. The overall Gibbs energy profile for cyclohexene substrate were shown in Figure S26. Given that the subsequent ligand-assisted β -H elimination for *Z*-allylation (**cy-ts-7a**) was 6.3 kcal mol⁻¹ higher than the rotational barrier (**cy-ts-6a**), we estimate

that the barriers for both *E*-allylation and styrenylation are at least ~20 kcal mol⁻¹ higher than *Z*-allylation (**cy-ts-7a**), thus being disfavoured by 1 in a trillion. Therefore, if at all, only *Z*-allylated product can be formed using cyclohexene substrate.

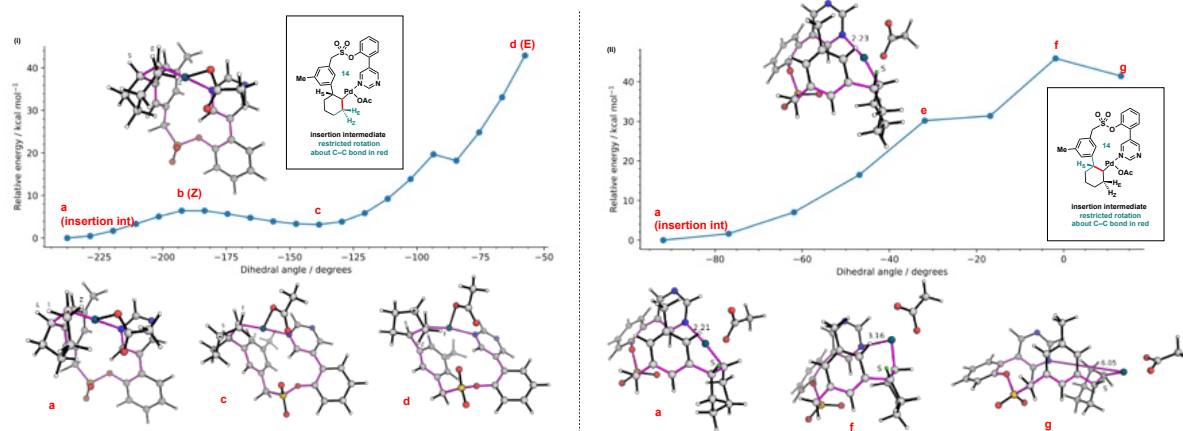


Figure S25. Dihedral angle scan (about C–C bond in red) for rotational barrier for the formation of (i) *E*-/*Z*-allylated products and (ii) styrenyl product for cyclohexene substrate.

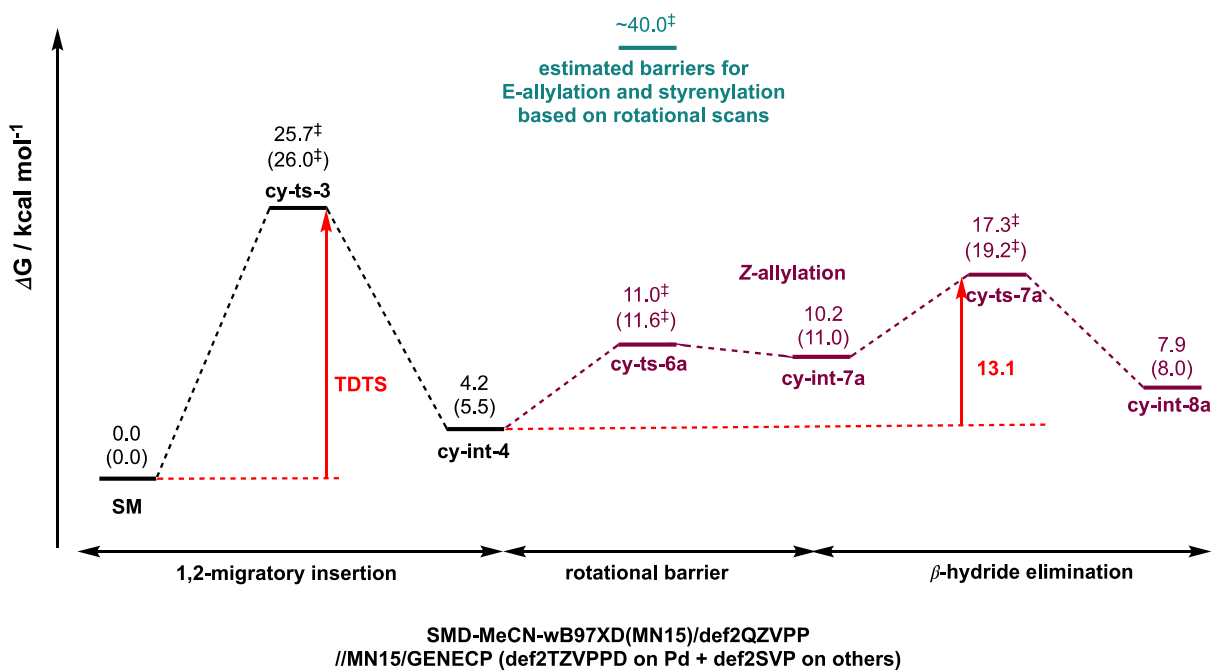


Figure S26. Gibbs free energy profile for *Z*-allylation using cyclohexene substrate. **cy-ts-3** is the same as **cy-d1-c1** as in Figure S20(e).

2.9.10 Absolute energies, zero-point energies

Absolute values (in Hartrees) for SCF energy, zero-point vibrational energy (ZPE), enthalpy and quasi-harmonic Gibbs free energy (at 363K) for optimised structures are given below. For harmonic frequency analysis, a plus (+) sign indicates that the lowest frequency of the optimised energy minimal structures is positive, and single negative frequency for each transition state is included. Single point corrections in SMD acetonitrile using ω B97X-D and MN15 functionals are also included. Each sub-heading corresponds to a subfolder inside the *structures_xyz* folder where all optimised structural coordinates are given in .xyz format, along with the corresponding (gas-phase) energy, *E*.

Structure	E/au	ZPE/au u	H/au	qh-G/au	Im.Freq/ cm ⁻¹	SP ω B97X-D (MeCN)	SP MN15 (MeCN)
0. Starting materials:							
arene	-	0.3115	-	-	-	-	-
1a	1426.522 9	09	1426.180 7	1426.269	+	1429.0622721 6	1428.691971 5
trans-	-	0.1651	-	-	-	-	-
hexen	235.3139 9	1	235.1364 5	235.1857 7	+	-235.88622142 -235.7628220	-235.7628220
cis-	-	0.1654	-	-	-	-	-
hexen	235.3122 6	29	235.1344 6	235.1835 2	+	-235.88455969 -235.7610397	-235.7610397
cyclo-	-	0.1463	-	-	-	-	-
hexen	234.1283 2	25	233.9727 3	234.0146 6	+	-234.68105898 -234.5687484	-234.5687484

HOA	-	0.0621	-	-	-	+	-229.13726389	-229.0706003
c	228.6445	97	228.5750	228.6124	-	-	-	-
N-								
acetyl	-	0.2314	-	-	-	-	-	-
-	593.1581	35	592.9054	592.9754	+	-	-594.47065223	-594.2582931
norle	9	-	8	6	-	-	-	-
ucine	-	-	-	-	-	-	-	-
Pd(OAc)₂	-	0.1043	-	-	-	+	-585.03620367	-584.6482919
	583.8099	26	583.6901	583.7484	-	-	-	-
	3	-	2	8	-	-	-	-
Pd₃(OAc)₆	-	0.3178	-	-	-	+	-	-
	1751.587	68	1751.221	1751.347	-	-	-	-
	3	-	8	2	-	-	-	-
1. meta-allylation:								
int-1	-	0.4173	-	-	-	-	-	-
	2010.361	36	2009.896	2010.018	+	-	-	-
	-	-	6	7	-	-	-	-
ts-1	-	0.4119	-	-	-	-	-	-
	2010.336	75	2009.877	2009.998	-	-	-	-
	1	-	4	9	1136.100	2014.0948740	2013.332751	5
int-2	-	0.4172	-	-	-	-	-	-
	2010.351	56	2009.886	2010.010	+	-	-	-
	5	-	8	3	-	-	-	-

int-1'	2146.206	0.5229	-	2145.631	-	2145.763	+	2150.3058485	-2149.465115
	8	38		5				4	
ts-1'	2146.190	0.5178	-	2145.621	2145.751	1275.114	-	2150.2850861	-2149.445114
	9	66		2	8	7		0	
int-2'	2146.215	0.5236	-	2145.639	-	2145.771	+	2150.3093651	-2149.472983
	2	42		2				5	
int-3	2017.031	0.5210	-	2016.458	2016.590	+	-	2020.8726358	2020.056335
	4	84			4			8	5
ts-3	2017.015	0.5202	-	2016.443	2016.574	-	-	2020.8571594	-2020.04
	3	4		9	2	281.0309		6	
int-4	2017.054	0.5225	-	2016.481	2016.610	+	-	2020.8951539	-2020.078034
	6	03			2			7	
ts-4	2017.039	0.5205	-	2016.468	2016.595	-95.8045	-	2020.8725658	-2020.056365
	5	7		5	9			1	
int-5	2017.042	0.5207	-	2016.470	2016.599	+	-	2020.8761334	-2020.059231
	4	22		5	5			5	

ts-5	-	2017.037	0.5184	-	2016.468	2016.596	-	534.1546	-	2020.8694761	-2020.053557
		6	43		4	3			2		
int-6	-	2017.048	0.5198	-	2016.477	2016.606	+		-	2020.8814551	-2020.065211
		7	9		5	8			4		
int-7	-	2017.047	0.5209	-	2016.475	2016.605	+		-	2020.8896222	-2020.069785
		9	31		9	3			6		
ts-7	-	2017.043	0.5169	-	2016.475	2016.603	-	960.7952	-	2020.8775839	-2020.058839
			19		4	8			4		
int-8	-	2017.065	0.5214	-	2016.492	2016.622	+		-	2020.8959791	-2020.079392
		1	65			8			2		
ts-7'	-	2017.016	0.5163	-	2016.448	-	-	975.0604	-	2020.8468038	-2020.030891
		5	98		5	2016.579			1		

2. Regioselectivity (Z-allylation vs styrenylation):

ts-4a	-	2017.037	0.5211	-	2016.465	2016.592	-77.2317		-	2020.8707224	-2020.05477
		2	16		9	7			4		
int-5a	-	2017.039	0.5211	-	2016.466	2016.595	+		-	2020.8730736	-2020.056043
		1	07		9	6			1		

ts-5a	2017.033 9	0.5184 58	-	2016.464 8	2016.592 6	-	516.2140	-	2020.8663071 8	-2020.049971
int-6a	2017.045 6	0.5199 94	-	2016.474 3	2016.603 6	-	+	-	2020.8797064 2	-2020.062662
ts-7a	2017.040 3	0.5172 41	-	2016.472 5	2016.600 6	-	-	-	2020.8747277 9	-2020.056175
ts-4b	2017.019 5	0.5206 51	-	2016.448 3	2016.576 3	-	-49.4039	-	2020.8627730 3	-2020.045129
int-5b	-	0.5203 8	-	2016.451 3	2016.581 2	-	+	-	2020.8663448 6	-2020.04869
ts-5b	2017.023 3	0.5175 49	-	2016.454 2	2016.585 2	-	-	-	2020.8604659 9	-2020.044136
int-6b	2017.027 2	0.5189 73	-	2016.456 4	2016.587 4	-	+	-	2020.8603052 0	-2020.047355
ts-7b	2016.985 3	0.5138 83	-	2016.419 9	2016.549 9	-	-1493.046 9	-	2020.8110423 8	-2019.995037

3. Ligand identity in TDTS:

ts-3-	-	2017.015	0.5202	2016.443	2016.574	281.0309	-2020.85716
Ac-c1	35	4	89	18	0		-2020.03997
ts-3-	-	2017.012	0.5200	2016.441	2016.571	286.4834	-2020.85668
Ac-c2	91	6	55	93	0		-2020.03961
ts-3-	-	2017.010	0.5201	2016.439	2016.570	284.0324	-2020.85518
Ac-c3	98	7	44	63	0		-2020.03759
ts-3-	-	2017.012	0.5201	2016.441	2016.571	305.7022	-2020.85540
Ac-c4	57	3	08	53	0		-2020.03868
ts-3-	-	2017.002	0.5201	2016.430	2016.560	296.0877	-2020.85451
Ac-c5	08	5	87	47	0		-2020.03664
ts-3-	-	2017.002	0.5201	2016.431	2016.560	295.2832	-2020.85081
Ac-c6	34	1	16	56	0		-2020.03394
ts3' -b -aa-c1	-	2381.537	0.6894	-	-	-	-
	3	22		2380.782	2380.942	284.2484	2386.1978885
ts3' -b -aa-c2	-	2381.537	0.6895	-	-	-	-
	8	07		2380.783	2380.940	283.7738	2386.1972974
				2	7	2	2

ts3' _b	-	0.6891	-	-	-	-	-
-aa-c3	2381.532 2	98	2380.777 5	-2380.9	283.7067	2386.1955226 0	-2385.2316
ts3' _b	-	0.6895	-	-	-	-	-
-aa-c4	2381.535 5	09	2380.780 7	-2380.94	281.9868	2386.1959698 2	-2385.2323
ts3' _b	-	0.6892	-	-	-	-	-
-aa-c5	2381.532 1	92	2380.777 4	2380.936 9	304.8330	2386.1946542 6	-2385.2314
ts3' _b	-	0.6893	-	-	-	-	-
-aa-c6	2381.535 7	62	2380.781 2	-2380.9	269.5971	2386.1950421 6	-2385.2323
ts3' _b	-	0.6894	-	-	-	-	-
-aa-c7	2381.531 3	85	2380.776 5	-2380.9	281.9394	2386.1943224 0	-2385.23
ts3' _b	-	0.6896	-	-	-	-	-
-aa-c8	2381.535 2	71	2380.780 3	2380.938 6	303.3393	2386.1923800 4	-2385.2307
ts3' _b	-	0.6898	-	-	-	-	-
-aa-c9	2381.531 5	67	2380.776 6	2380.934 6	298.0564	2386.1915142 5	-2385.2285
ts3' _b	-	0.6896	-	-	-	-	-
-aa-c10	2381.539 8	94	2380.785 2	2380.942 1	273.9343	2386.1922180 4	-2385.2285

ts3'_b	-	0.6898	-	-	-	-	-	-
-aa-	2381.538	9	2380.783	2380.939	301.0522	2386.1899442	-2385.2285	
c11			3	5		8		

ts3'_b	-	0.6897	-	-	-	-	-	-
-aa-	2381.537	51	2380.782	2380.939	281.9361	2386.1901799	-2385.2268	
c12	3		5	7		8		

3. Ligand non-participation in C–H activation and insertion:

ts-1'a	2146.150	0.5181	-	-	-	-	-	-
		13	2145.580	2145.711	436.6324	2150.2517966	-2149.412069	
	6		5	9		3		

ts-1'b	2374.853	0.5819	-	-	-	-	-	-
		88	2374.211	2374.360	1144.373	2379.4260737	2378.518059	
	4		4	9		3		2

ts-1'c1	2374.859	0.5813	-	-	-	-	-	-
		02	2374.217	2374.366	1121.517	2379.4343307	2378.527017	
	1		3	4	4	9		9

ts-1'c2	2374.862	0.5816	-	-	-	-	-	-
		18	2374.220	2374.368	1158.865	2379.4322103	2378.524855	
	2		2	8	0	7		8

ts-1'c3	2374.864	0.5818	-	-	-	-	-	-
		42	2374.222	2374.370	1167.889	2379.4311132	2378.523873	
	4		3	6	9	8		6

ts-1'c4	2374.857	0.5818	-	-	-	-	-	-
		3	2374.215	2374.363	1158.697	2379.4280753	2378.519836	
			1	1	9	6		5

ts-1'c5	-	2374.839	0.5817	-	2374.198	2374.345	1119.736	2379.4117375	2378.504226
	9	15		2	5		2	3	6

4. Arene site selectivity (*ortho*- vs *para*-):

ts-1o	-	2010.327	0.4123	-	2009.868	2009.989	1136.403	2014.0809551	2013.322784
	2	35		4	4		8	2	8
ts-1o-c2	-	2010.326	0.4127	-	2009.867	2009.987	-	2014.0754951	2013.317891
	4	28		5	3	974.1986		4	6
ts-1o'	-	2146.191	0.5181	-	2145.621	2145.753	1079.014	2150.2836752	-2149.445889
	6	62		7	1		6	5	
ts-3o	-	2017.002	0.5204	-	2016.430	2016.560	-	2020.8357802	-2020.021731
	5	45		9	9	330.9693		2	
int-4o	-	2017.037	0.5230	-	2016.463	2016.591	+	2020.8678039	-2020.052957
	3	08		3	9			5	
ts-1p	-	2010.335	0.4121	-	2009.877	2009.998	1147.996	2014.0921925	2013.332518
	9	69		2	4		6	9	6
ts-1p-c2	-	2010.337	0.4123	-	2009.878	2009.999	1129.467	2014.0909101	2013.332141
	3	06		7	2		5	4	8

ts-1p'	2146.181	0.5182	-	2145.611	2145.742	-	744.9454	-	2150.2710257	-2149.431512
			9		2	5			2	
	4									
ts-3p	2017.011	0.5207	-	2016.439	2016.568	-	-293.7	-	2020.8506834	-2020.036795
			13		9	8			1	
	5									
int-4p	2017.046	0.5229	-	2016.472	2016.601	-	+	-	2020.8846075	-2020.068617
			73		5	4			0	
	4									

5. Boltzmann sampling for 1,2-migratory**insertion:**

trans-d1-c1	2017.012	0.5201	-	2016.441	2016.571	-	-	-	2020.8554024	-2020.038678
			25		1	5			9	
	6									
trans-d1-c2	2017.014	0.5201	-	2016.442	2016.572	-	-	-	2020.8556619	-2020.039368
			58		8	8			3	
	2									
trans-d1-c3	2017.012	0.5198	-	2016.441	2016.571	-	-	-	2020.8532857	2020.037741
			17		2	6			9	
	3									
trans-d1-c4	2017.012	0.5200	-	2016.441	2016.571	-	-316.8	-	2020.8530009	-2020.036383
			1		2	8			1	
	6									

trans-	-						-	
d1-c5	2017.014 9	0.5204 54	-	2016.443 4	2016.572 8	-316.9	2020.8539279 1	-2020.037906
trans-	-	0.5197	-	2016.437 3	-	2016.568 317.3912	2020.8522987 7	-2020.034701
d1-c6	2017.008 5	82						
trans-	-	0.5205	-	2016.442 8	2016.572 5	-	2020.8530853 6	-2020.037854
d1-c7	2017.014 4	09				315.0322		
trans-	-	0.5208	-	2016.445 3	2016.573 6	-	2020.8536826 7	-2020.038209
d1-c8	2017.016 8	16				311.5392		
trans-	-	0.5198	-	2016.438 3	2016.568 5	-	2020.8490570 4	-2020.033366
trans-	-	0.5196	-	2016.443 1	2016.573 3	-	-2020.85718	-2020.040593
d2-c1	2017.014 1	63				282.5387		
trans-	-	0.5196	-	2016.444 7	2016.573 7	-	-2020.856582	-2020.040347
d2-c2	2017.014 9	12				308.8734		
trans-	-	0.5202	-	-	-	-	2020.8566662 6	-2020.040614
d2-c3	2017.017 3	44		2016.446	2016.575	288.8986		

<i>trans-</i> d2-c4	-	0.5203	-	2016.446	-	2016.575	-	304.4657	-2020.855951	-2020.040502
	8		81		5					
<i>trans-</i> d2-c5	-	0.5198	-	2016.441	-	2016.571	-	282.6224	-2020.8542	-2020.037271
	8		58		6		4			
<i>trans-</i> d2-c6	-	0.5198	-	2016.443	-	2016.572	-	284.4537	-2020.854195	-2020.038113
	6		44		6		9			
<i>trans-</i> d2-c7	-	0.5198	-	2016.44	-	2016.570	-	262.2307	2020.8531970	-2020.037409
	1		6			1			9	
<i>trans-</i> d2-c8	-	0.5197	-	2016.443	-	2016.573	-	303.2176	-2020.853935	-2020.038479
	7		73		8					
<i>trans-</i> d2-c9	-	0.5201	-	2016.439	-	2016.568	-	258.7607	2020.8509175	-2020.035064
	5		14		3		8		9	
<i>cis-</i> d1-c1	-	0.5197	-	2016.440	-	2016.570	-	293.1446	2020.8545480	-2020.038653
	4		7		3		6		9	
<i>cis-</i> d1-c2	-	0.5202	-	2016.443	-	2016.572	-	289.5588	2020.8546081	-2020.038579
	3		43			3			5	

<i>cis-</i> d1-c3	-	2017.009 4	0.5198 8	-	2016.438 1	2016.568 6	-	305.4801 -	2020.8529871 9	-2020.036652
<i>cis-</i> d1-c4	-	2017.012 8	0.5202 44	-	2016.441 4	-	2016.571 -	296.5738 -	2020.8540071 6	-2020.037311
<i>cis-</i> d1-c5	-	2017.013 2	0.5200 84	-	2016.442 1	2016.571 3	-	287.1232 -	2020.8534278 3	-2020.038021
<i>cis-</i> d1-c6	-	2017.012	0.5201 64	-	2016.441 8	2016.568 8	-	295.7306 -	2020.8532794 5	-2020.037221
<i>cis-</i> d1-c7	-	2017.012	0.5207 87	-	2016.440 5	2016.568 9	-	300.2449 -	2020.8480517 7	-2020.033502
<i>cis-</i> d1-c8	-	2017.010 3	0.5208 06	-	2016.438 6	2016.567 4	-	308.1908 -	2020.8478232 8	-2020.03263
<i>cis-</i> d1-c9	-	2017.005 1	0.5211 4	-	2016.433 3	2016.561 8	-	314.0032 -	2020.8401955 6	-2020.025393
<i>cis-</i> d2-c1	-	2017.010 3	0.5201 14	-	2016.438 9	2016.569 1	-	298.4609 -	2020.8528853 9	-2020.037075

<i>cis-</i> d2-c2	-	2017.010 9	0.5204 54	-	2016.439 3	2016.569 1	-	300.5416 6	2020.8532499 6	-2020.03695
<i>cis-</i> d2-c3	-	2017.012 4	0.5204 31	-	2016.441 1	2016.570 2	-	287.7811 4	2020.8536031 4	-2020.038019
<i>cis-</i> d2-c4	-	2017.011 7	0.5201 84	-	2016.440 4	2016.570 2	-	300.4347 6	2020.8521707 6	-2020.037598
<i>cis-</i> d2-c5	-	2017.010 1	0.5203 28	-	2016.438 6	2016.568 7	-	309.4578 3	2020.8515561 3	-2020.036441
<i>cis-</i> d2-c6	-	2017.007 9	0.5202 58	-	2016.436 4	2016.566 7	-	313.6194 3	2020.8512690 3	-2020.034999
<i>cis-</i> d2-c7	-	2017.008 2	0.5203 27	-	2016.436 8	2016.565 7	-	-296.732 2	2020.8498942 2	-2020.033341
<i>cis-</i> d2-c8	-	2017.003 6	0.5207 16	-	2016.431 9	2016.561 5	-	311.8461 5	2020.8461443 5	-2020.028735
<i>cis-</i> d2-c9	-	2017.002 8	0.5206 98	-	2016.431 1	2016.560 6	-	316.5124 0	2020.8444883 0	-2020.028321

cy-d1-c1	-	2015.824	0.5009	-	2015.275	2015.399	-	309.5106	-	2019.6462757	-2018.840491
	5		39		2	7			0		
cy-d1-c2	-	2015.823	0.5013	-	2015.273	-	2015.398	-	314.2776	-	2019.6457994
	3		42		7					2	-2018.839852
cy-d1-c3	-	2015.826	0.5012	-	2015.277	2015.400	-	-	301.2641	-	2019.6445767
	6		53		1	6				2	-2018.840282
cy-d1-c4	-	2015.821	0.5013	-	2015.271	2015.395	-	-	292.1391	-	2019.6428992
	07		07		2	6				9	-2018.83771
cy-d2-c1	-	2015.823	0.5009	-	2015.274	2015.397	-	-304.458	-	2019.6457031	-2018.839656
	6		56		4	8				0	
cy-d2-c2	-	2015.825	0.5009	-	2015.276	2015.399	-	-291.53	-	2019.6448124	-2018.840874
	2		5			3				2	
cy-d2-c3	-	2015.819	0.5008	-	2015.269	2015.394	-	-	276.5101	-	2019.6439305
	3		87		8	1				1	-2018.838106
cy-d2-c4	-	2015.822	0.5010	-	2015.273	2015.396	-	-	303.1028	-	2019.644799
	5		28		3	5					2018.838686
											55

6. Isodesmic studies:

pyridine	-	0.0894	-	-	-	+	-248.30904588	-248.2228936
	247.7627	6	73	247.6659	6	247.7041		
						1		
ts-3-isoo	-	0.6108	-	-	-	-	-	-
	2264.788	5	71	2264.117	5	2264.267	325.2881	2269.1677108
						2		-2268.26553
ts-3o-isoo	-	0.6118	-	-	-	-	-	-
	2264.803	6	69	2264.132	7	2264.277	285.3699	2269.1666541
						6		-2268.26716
ts-3p-isoo	-	0.6116	-	-	-	-	-	-
	2264.794	2	33	2264.123	8	2264.270	310.8723	2269.1700187
						8		-2268.27014

7. <i>cis</i>-hexene product selectivity:								
cis-int-4	-	0.5222	-	-	-	-	-	-
	2017.049	1	86	2016.475	5	2016.605	+	2020.8908183
cis-ts-6	-	0.5221	-	-	-	-	-	-
	2017.047	7	16	2016.475	3	2016.602	-56.3933	2020.8881911
						6		-2020.071351
cis-int-7	-	0.5218	-	-	-	-	-	-
	2017.045	8	79	2016.473	3	2016.600	+	-2020.878591
cis-ts-7	-	0.5176	-	-	-	-	-	-
	-2017.04	15	1	2016.472	9	2016.598	894.6881	2020.8699586
						9		-2020.051674
							6	

<i>cis</i> -int-8	-	2017.065	0.5221	-	2016.491	2016.621	+	2020.8893887	2020.073698
	2		18	8		1	0		04
<i>cis</i> -ts-6a	-	2017.038	0.5224	-	2016.465	2016.593	-99.8893	2020.8792089	-2020.061699
	5		31	9		1	8		
<i>cis</i> -int-7a	-	2017.039	0.5218	-	2016.467	2016.594	+	2020.8770836	-2020.058029
	4		02		5		8		
<i>cis</i> -ts-7a	-	2017.034	0.5180	-	2016.466	2016.592	-978.8647	2020.8649285	-2020.046586
	6		17	5		8	9		
<i>cis</i> -int-8a	-	2017.060	0.5228	-	2016.486	2016.614	+	2020.8851595	-2020.069733
	4		8	6		9	8		
<i>cis</i> -ts-4b	-	2017.016	0.5205	-	2016.445	2016.573	-82.2613	2020.8602446	-2020.041432
	3		14		9		6		
<i>cis</i> -int-5b	-	2017.034	0.5203	-	2016.462	2016.593	+	2020.8734714	-2020.056019
	2		72	2		0	1		
<i>cis</i> -ts-5b	-	2017.029	0.5178	-	2016.459	2016.589	-366.9912	2020.8643520	-2020.049118
			17	9		8	8		

<i>cis</i> -int-6b	-	2017.031	0.5189	-	2016.461	2016.591	+	2020.8635495	-2020.05077
		8	39		1	8		5	

<i>cis</i> -ts-5b-c2	-	2017.015	0.5180	-	2016.446	2016.575	-	2020.8542316	-2020.038656
		8	3		8	6	480.8873	6	

8. cyclohexene product selectivity:

cy-int-4	-	2015.863	0.5032	-	2015.312	2015.435	+	2019.6837660	-2018.876402
		9	7		3	8		1	

cy-ts-6a	-	2015.859	0.5033	-	2015.308	2015.429	-88.5455	2019.6741799	-2018.868046
		1	92		4	7		0	

cy-int-7a	-	2015.859	0.5025	-	2015.308	2015.431	+	2019.6741475	-2018.867609
		1	39		4	1		5	

cy-ts-7a	-	2015.847	0.4985	-	2015.301	2015.422	1032.925	2019.6597835	-2018.851573
		7	27		7	7	6	8	

cy-int-8a	-	2015.871	0.5032	-	2015.320	2015.443	+	2019.6780552	-2018.872553
		7	44		1	5		2	

2.9.11 Optimized geometries

Geometries of all optimized structures (in .xyz format with their associated energy in Hartrees) are included in a separate folder named *structures_xyz* with an associated README file. All these data have been deposited with this Supporting Information and uploaded to zenodo.org (DOI: 10.5281/zenodo.2775841).

3. References:

Full reference for ref (1):

Gaussian 16, Revision A.01, Frisch, M. J.; Trucks, G. W.; Schlegel, H. B.; Scuseria, G. E.; Robb, M. A.; Cheeseman, J. R.; Scalmani, G.; Barone, V.; Mennucci, B.; Petersson, G. A.; Nakatsuji, H.; Caricato, M.; Li, X.; Hratchian, H. P.; Izmaylov, A. F.; Bloino, J.; Zheng, G.; Sonnenberg, J. L.; Hada, M.; Ehara, M.; Toyota, K.; Fukuda, R.; Hasegawa, J.; Ishida, M.; Nakajima, T.; Honda, Y.; Kitao, O.; Nakai, H.; Vreven, T.; Montgomery Jr., J. A.; Peralta, J. E.; Ogliaro, F.; Bearpark, M.; Heyd, J. J.; Brothers, E.; Kudin, K. N.; Staroverov, V. N.; Kobayashi, R.; Normand, J.; Raghavachari, K.; Rendell, A.; Burant, J. C.; Iyengar, S. S.; Tomasi, J.; Cossi, M.; Rega, N.; Millam, J. M.; Klene, M.; Knox, J. E.; Cross, J. B.; Bakken, V.; Adamo, C.; Jaramillo, J.; Gomperts, R.; Stratmann, R. E.; Yazyev, O.; Austin, A. J.; Cammi, R.; Pomelli, C.; Ochterski, J. W.; Martin, R. L.; Morokuma, K.; Zakrzewski, V. G.; Voth, G. A.; Salvador, P.; Dannenberg, J. J.; Dapprich, S.; Daniels, A. D.; Farkas, Ö.; Foresman, J. B.; Ortiz, J. V.; Cioslowski, J.; Fox, D. J. Gaussian, Inc., Wallingford CT, 2016.

- (1) Frisch, M. J.; Trucks, G. W.; Schlegel, H. B.; Scuseria, G. E.; Robb, M. A.; Cheeseman, J. R.; Scalmani, G.; Barone, V.; Mennucci, B.; Petersson, G. A.; et al. Gaussian 16, Revision A.01. 2016.
- (2) Yu, H. S.; He, X.; Li, S. L.; Truhlar, D. G. MN15: A Kohn–Sham Global-Hybrid Exchange–Correlation Density Functional with Broad Accuracy for Multi-Reference and Single-Reference Systems and Noncovalent Interactions. *Chem. Sci.* **2016**, 7 (8), 5032–5051.

- (3) Andrae, D.; Häußermann, U.; Dolg, M.; Stoll, H.; Preuß, H. Energy-Adjustedab Initio Pseudopotentials for the Second and Third Row Transition Elements. *Theor. Chim. Acta* **1990**, *77* (2), 123–141.
- (4) Weigend, F.; Ahlrichs, R. Balanced Basis Sets of Split Valence{,} Triple Zeta Valence and Quadruple Zeta Valence Quality for H to Rn: Design and Assessment of Accuracy. *Phys. Chem. Chem. Phys.* **2005**, *7* (18), 3297–3305.
- (5) Weigend, F. Accurate Coulomb-Fitting Basis Sets for H to Rn. *Phys. Chem. Chem. Phys.* **2006**, *8* (9), 1057–1065.
- (6) Mekareeya, A.; Walker, P. R.; Couce-Rios, A.; Campbell, C. D.; Steven, A.; Paton, R. S.; Anderson, E. A.; Ross Walker, P.; Couce-Rios, A.; Campbell, C. D.; et al. Mechanistic Insight into Palladium-Catalyzed Cycloisomerization: A Combined Experimental and Theoretical Study. *J. Am. Chem. Soc.* **2017**, *139* (29), 10104–10114.
- (7) Deb, A.; Hazra, A.; Peng, Q.; Paton, R. S.; Maiti, D. Detailed Mechanistic Studies on Palladium-Catalyzed Selective C–H Olefination with Aliphatic Alkenes: A Significant Influence of Proton Shuttling. *J. Am. Chem. Soc.* **2017**, *139* (2), 763–775.
- (8) Chai, J.-D.; Head-Gordon, M. Long-Range Corrected Hybrid Density Functionals with Damped Atom-Atom Dispersion Corrections. *Phys. Chem. Chem. Phys.* **2008**, *10* (44), 6615–6620.
- (9) Marenich, A. V; Cramer, C. J.; Truhlar, D. G. Universal Solvation Model Based on Solute Electron Density and on a Continuum Model of the Solvent Defined by the Bulk Dielectric Constant and Atomic Surface Tensions. *J. Phys. Chem. B* **2009**, *113* (18), 6378–6396.
- (10) Grimme, S. Supramolecular Binding Thermodynamics by Dispersion-Corrected Density Functional Theory. *Chem. – A Eur. J.* **2012**, *18* (32), 9955–9964.
- (11) Funes-Ardoiz, I.; Paton, R. S. GoodVibes v1.0.1 <http://doi.org/10.5281/zenodo.56091>.
- (12) E. D. Glendening, A. E. Reed, J. E. Carpenter, and F. W. NBO Version 3.1.,
- (13) Contreras-García, J.; Johnson, E. R.; Keinan, S.; Chaudret, R.; Piquemal, J.-P.; Beratan,

- D. N.; Yang, W. NCIPLOT: A Program for Plotting Noncovalent Interaction Regions. *J. Chem. Theory Comput.* **2011**, *7* (3), 625–632.
- (14) Sosa, C.; Andzelm, J.; Elkin, B. C.; Wimmer, E.; Dobbs, K. D.; Dixon, D. A. A Local Density Functional Study of the Structure and Vibrational Frequencies of Molecular Transition-Metal Compounds. *J. Phys. Chem.* **1992**, *96* (16), 6630–6636.
- (15) Godbout, N.; Salahub, D. R.; Andzelm, J.; Wimmer, E. Optimization of Gaussian-Type Basis Sets for Local Spin Density Functional Calculations. Part I. Boron through Neon, Optimization Technique and Validation. *Can. J. Chem.* **1992**, *70* (2), 560–571.
- (16) Schrödinger, LLC. *The {PyMOL} Molecular Graphics Development Component, Version~1.8*; 2015.
- (17) Maji, A.; Guin, S.; Feng, S.; Dahiya, A.; Singh, V. K.; Liu, P.; Maiti, D. Experimental and Computational Exploration of Para-Selective Silylation with a Hydrogen-Bonded Template. *Angew. Chemie - Int. Ed.* **2017**, *56* (47), 14903–14907.
- (18) Maji, A.; Dahiya, A.; Lu, G.; Bhattacharya, T.; Brochetta, M.; Zanoni, G.; Liu, P.; Maiti, D. H-Bonded Reusable Template Assisted Para-Selective Ketonisation Using Soft Electrophilic Vinyl Ethers. *Nat. Commun.* **2018**, *9* (1).
- (19) Wheeler, S. E.; Houk, K. N.; Schleyer, P. V. R.; Allen, W. D. A Hierarchy of Homodesmotic Reactions for Thermochemistry. *J. Am. Chem. Soc.* **2009**, *131* (7), 2547–2560.
- (20) Wheeler, S. E. Homodesmotic Reactions for Thermochemistry. *Wiley Interdisciplinary Reviews: Computational Molecular Science*. 2012, pp 204–220.
- (21) Peng, Q.; Duarte, F.; Paton, R. S. Computing Organic Stereoselectivity - from Concepts to Quantitative Calculations and Predictions. *Chem. Soc. Rev.* **2016**, *45* (22), 6093–6107.
- (22) Fang, L.; Saint-Denis, T. G.; Taylor, B. L. H.; Ahlquist, S.; Hong, K.; Liu, S.; Han, L.; Houk, K. N.; Yu, J. Q. Experimental and Computational Development of a Conformationally Flexible Template for the Meta-C-H Functionalization of Benzoic Acids. *J. Am. Chem. Soc.* **2017**, *139* (31), 10702–10714.

4. Author Contributions

T.K.A. and R.M. conceived and developed the palladium catalyzed *meta*-selective C–H allylation. T.K.A. and R.M. optimized the reaction conditions. TKA, M.S.S., S.M. and N.P. prepared the starting materials and identified the substrates scope. TKA and M.S. conducted the mechanistic investigations. X.Z. designed and performed the computational studies. R.S.P supervised the computational studies. D.M. supervised the project. T.K.A. and X.Z. wrote the manuscript with input from R.S.P. and D.M. All authors read and commented on the manuscript.